The Design & Construction of a Proton Microprobe Using a GE PETtrace Cyclotron

---

A Thesis

presented to

the Faculty of the Graduate School

at the University of Missouri-Columbia

In Partial Fulfillment

of the Requirements for the Degree

Master of Science

By

Michael S. Beumer

Dr. Patrick Pinhero, Thesis Supervisor

March 2012

The undersigned, Appointed by the Dean of the Graduate School, have examined the thesis entitled

The Design & Construction of a Proton Microprobe Using a GE PETtrace Cyclotron

Presented by

Michael S. Beumer

A candidate for the degree of

Master of Science

And hereby certify that in their opinion it is worthy of acceptance.

Dr. Patrick Pinhero ____

Dr. John Gahl ____

Dr. Paul Chan ____

Dr. David Robertson ____

Acknowledgements

First and foremost I would like to thank my friends and family for the unbound support they have shown me. Without your support I don't know where I'd be. Thank you for leading me out of the forest, that is graduate school, and finding my way home.

I wish to express a sincere appreciation for Dr. John Gahl for taking me under his wing and mentoring me, providing me with direction, and helping me obtain this degree. I value your advice and am very thankful that you were a part of my graduate studies.

I would like to thank Dr. Paul Chan, Dr. Mary Meyers, Dr. David Retzloff, and Dr. Stephen Lombardo for all of your support and mentoring throughout my graduate career. Thank you for being a light in some of the dark days of graduate school and guiding me through.

I want to thank my committee members, Dr. Patrick Pinhero, Dr. John Gahl, Dr. Paul Chan, and Dr. David Robertson for working with me to obtain this degree. I also wish to thank Dr. Bill Miller, who was not a committee member, but worked closely with me on this project.

A special thanks to Alex Saale who was not just the cyclotron operator, but also a mentor who helped me keep this project going. Thank you for helping me navigate the MURR system. I would like to thank everyone at MURR, each of you were kind and helpful!

I wish to express my sincere thanks to the Department of Energy, Nuclear Engineering University programs, for funding my research and making this thesis possible.

The Design & Construction of a Proton Microprobe Using a GE PETtrace Cyclotron

Michael S. Beumer

Abstract

The interaction of fast neutrons with nuclear materials is a topic of fundamental interest in nuclear engineering. Fast neutrons possess the ability to degrade, and in some cases destroy, materials used in nuclear reactor pressure vessels and core internals. Unfortunately, there are very few facilities where extreme fast neutron fluences, approximately 300 displacements per atom, can be reasonably achieved. Research at the University of Missouri Research Reactor (MURR) Cyclotron has focused on increasing the fast neutron flux density by creating a very tight microspot.

This thesis focuses on characterizing the MURR cyclotron beam through accurate measurements using a radiochromic film technique, originally developed by Avila-Rodriguez.[1] An ion optics system was designed using SIMION, a finite element analysis software.[2] A quadrupole triplet was used to transport and focus the high-energy beam to a very small point.

A cyclotron-based beamline system was constructed at MURR with the following components: drift tubes, a sample chamber with appropriate vacuum components, and associated instrumentation. An acquisition computer and associated electronics were remotely positioned, outside of the cyclotron vault, to control the beamline and ion optics. This remote acquisition system includes a program to record beam current, sample chamber pressure, and the current supplied to the quadrupole magnets. Several safety interlocks were designed to protect workers and equipment. The construction, alignment, and startup of the beam line are presented. Preliminary irradiations of graphite with protons are also presented.

Table of Content

List of Figures

List of Tables

Chapter 1

Introduction

1.1 Introduction

A 16.5 MeV H+ micro-probe beamline is under construction at University of Missouri Research Reactor (MURR). The beamline will focus ions, accelerated from a GE PET-Trace cyclotron, to a point source, with currents up to 100 uA. An accurate estimation of the cyclotron beam is needed before optics can be designed. Measurement of the beam outlined by Avila-Rodriguez[1] was achieved using EBT2 Gafchromic film. Many heavy high energy microbeams have been designed over the years,[3] but none with the energy, current, and spot size described below. Focusing high-energy beams to a microspot is traditionally achieved using a quadrupole triplet.[3-4] SIMION was used[2b] to determine the quadrupole manufacturing parameters as well as the beamline size; it was also used to estimate the ion optics location along the beamline.

1.2 Charged Particle Optics

1.2.1 Electric & Magnetic Forces

A particle with charge ***q***, and velocity ***v*** is shown in Figure 1.1.

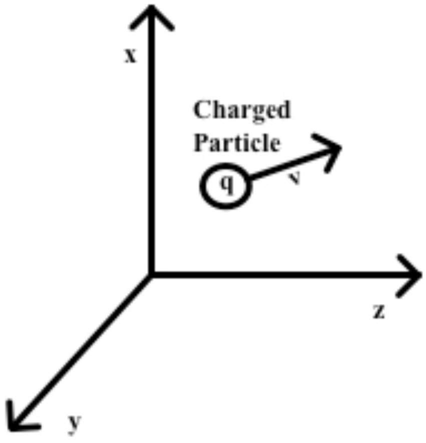

Figure 1.1 Velocity of a charged particle in Cartesian coordinates.

From Newton's first law we know the momentum $\boldsymbol{p}$ is defined by:

$$\boldsymbol{p} = \boldsymbol{m_p v} \tag{1.1}$$

where $\boldsymbol{m_p}$ is the rest mass of a proton. The momentum can be related to force $\boldsymbol{F}$ by Newton's second law:

$$\boldsymbol{F} = \boldsymbol{dp/dt} \tag{1.2}$$

The Lorentz force law states that the total force applied to a charged particle is given by

$$\boldsymbol{F} = \boldsymbol{q}(\boldsymbol{E} + \boldsymbol{v} \times \boldsymbol{B}) \tag{1.3}$$

where $\boldsymbol{E}$ is the electric field, and $\boldsymbol{B}$ is the magnetic field. The ion optics used in this research are magnetic and therefore $\boldsymbol{E}$ is negligible due to $\boldsymbol{B} >> \boldsymbol{E}$. The force term from cross product of the velocity of the charged particle and the magnetic field is orthogonal to the velocity and magnetic field vectors. Simplifying equation 1.3 yields:

$$F_x = q\left(v_y B_z - v_z B_y\right) \tag{1.4}$$

$$F_y = q(v_z B_x - v_x B_z) \tag{1.5}$$

$$F_z = q(v_x B_y - v_y B_x) \tag{1.6}$$

where the subscripts x, y, and z denote the components broken into Cartesian coordinates.

1.2.2 Particle Beam Background

Particle beams have a very high velocity in one direction and their velocity in the other directions are very small.[4] Ion beams always have a velocity component perpendicular to primary direction of motion.[4] The perpendicular velocity component of the ions can be attributed to the ion source; ion sources usually operate at high temperatures so the extracted ions will have a distribution of random thermal motion.[4] The ion source geometry could also have defects that cause the ions to accelerate differently.[4] Ion beam motions perpendicular to the beam can also be attributed to space charge effects.[4] . As a charged particle beam travels though space it expands, this expansion is known as beam divergence (see Figure 1.2). The divergence in the bending plane and across the bending plane are known as θ_b and θ_{ab}, respectively. The divergence 'in' the bending plane θ_b is larger than the divergence 'across' the bending plane due to the particles being bent in that plane. Ion lenses are needed to compress the charged particle beam that has expanded due to the existence of beam divergence. I will now introduce charged particle beam lenses so that we can understand how the B fields are created.

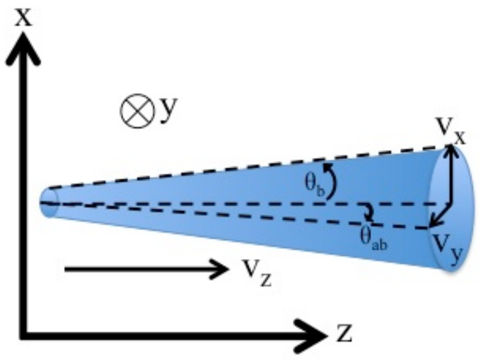

Figure 1.2 Diagram of the divergence of a charged particle beam.

1.2.3 General, Ion Optics

Charged particle beam lenses preform three important processes: beam confinement, beam focusing, and image formation.[4] Lenses confine the beam as it becomes larger due to the perpendicular velocity (see Figure 1.3a), which is important when transporting the beam long distances through small bores[4].

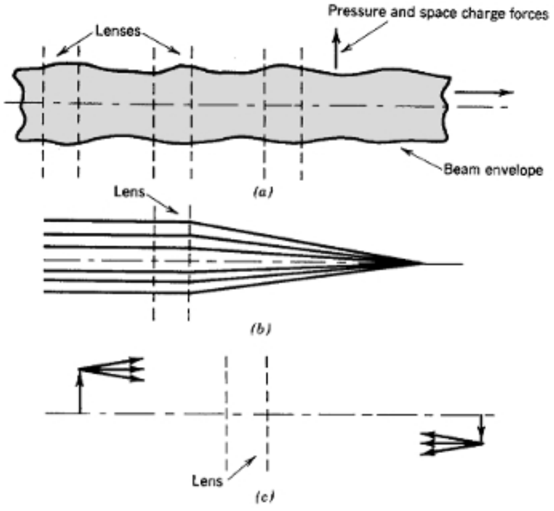

Figure 1.3 Functions of charged particle lenses. (a) Beam confinement. (b) Focusing to a spot. (c) Imaging.[4]

Lenses can focus the beam to a common spot (see Figure 1.3b), which leads to larger particle flux densities.[4] Lenses can also be used for imaging (see Figure 1.3c) when the particles fly through a lens the beam cross section is distorted. The distortion is a function of the lens, the particle beam masses, the particle beam charges, the particle beam velocities, and position of the individual particles in the beam. For example, a mass spectrometer lens sorts particles depending on their mass-to-charge ratio.

Magnetic quadrupole lenses are ideal for focusing charged particle beams. Quadrupole triplets are capable of focusing charged particle beams down to 1 um spot sizes.[3]

1.2.4 Magnetic Quadrupole Lens

A magnetic quadrupole lens is shown below in Figure 1.4.

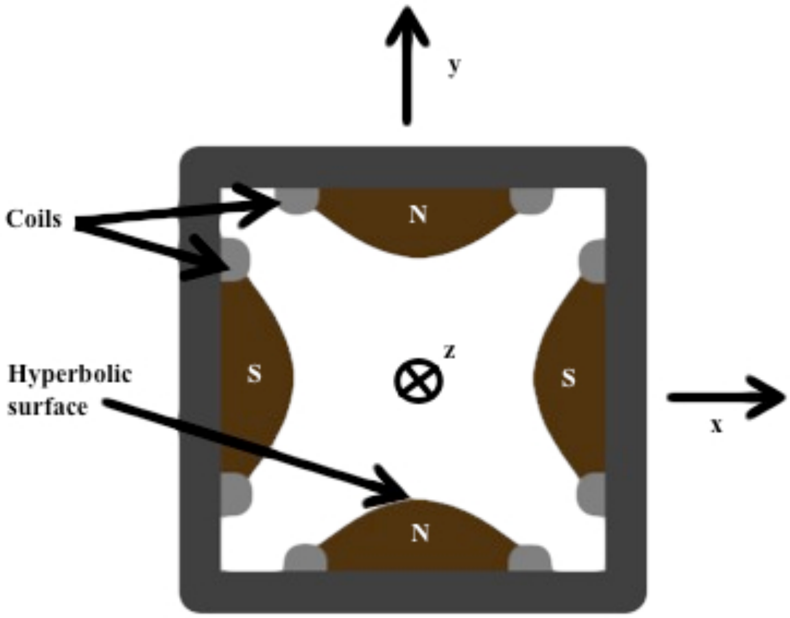

Figure 1.4 Electromagnetic quadrupole lens (cross section).

Current is driven through the coils, which creates the north and south poles as shown. The poles extend a length of $\boldsymbol{l}$ in the z-axis. The hyperbolic surface of a quadrupole is described by:

$$\frac{x^2}{a^2} - \frac{y^2}{a^2} = 1 \tag{1.7}$$

At the surface of the quadrupole, the magnetic field is assumed to be constant. Therefore, the boundary conditions needed to find the magnetic fields are:

$$\text{at } \frac{x^2}{a^2} - \frac{y^2}{a^2} = 1,\ B_x = B_o \tag{1.8}$$

$$\text{at } \frac{x^2}{a^2} - \frac{y^2}{a^2} = -1, B_y = B_o \tag{1.9}$$

$$\text{at } x = 0,\ y = 0,\ B = 0 \tag{1.10}$$

where B_o is the magnetic field at the surface of the pole closest to the axis and a is the minimum distance from the y-axis to the pole surface for equation 1.9 and from the x-axis to the pole surface for equation 1.10. The pole surfaces are parallel to the z-axis and therefore the magnetic field component in the z direction is:

$$B_z \approx 0 \tag{1.11}$$

This is not entirely true, because fringe fields exist outside of the yoke, but the contribution from the fringe fields will be ignored for these calculations. Static magnetic fields are described[4] by the Maxwell equations:

$$\nabla \cdot B = 0 \tag{1.12}$$

$$\boldsymbol{\nabla \times B = 0} \tag{1.13}$$

where the equation 1.12 and 1.13 can be rewritten in Cartesian coordinates to have the form:

$$\frac{d}{dx}B_x + \frac{d}{dy}B_y + \frac{d}{dz}B_z = 0 \tag{1.14}$$

$$[\frac{d}{dy}B_z - \frac{d}{dz}B_y]_x + [\frac{d}{dz}B_x - \frac{d}{dx}B_z]_y + [\frac{d}{dx}B_y - \frac{d}{dy}B_x]_z = 0 \tag{1.15}$$

Solving the Maxwell equations yields the magnetic field components:

$$B_x = B_o y/a \tag{1.16}$$

$$B_y = B_o x/a \tag{1.17}$$

1.2.5 Beam Transport Using a Magnetic Quadrupole Lens

The magnetic field components created by an electromagnetic quadrupole were derived in the previous section. The magnetic field components for a quadrupole are used in equation 1.4, equation 1.5, and equation 1.6 to find the force components:

$$F_x = q(v_z B_o x/a) \tag{1.18}$$

$$F_y = q(v_z B_o y/a) \tag{1.19}$$

$$F_z = q(v_x B_o x/a - v_y B_o y/a) \tag{1.20}$$

Let us assume that the charged particle in Figure 1.1 has the initial conditions:

$$at\ t = 0,\ v = v_0, x = x_0, y = y_0, z = z_0 \tag{1.21}$$

where the v_0 is the initial velocity, and $\boldsymbol{x_0}$, $\boldsymbol{y_0}$, and $\boldsymbol{z_0}$ is the position of the particle. Then velocity and position of the charged particle at any time is given by:

$$\boldsymbol{v_{x,t} = \int_0^t q\left(\frac{v_z B_o x}{a m_p}\right) dt + v_{x,0}} \tag{1.22}$$

$$\boldsymbol{v_{y,t} = \int_0^t q\left(\frac{v_z B_o y}{a m_p}\right) dt + v_{y,0}} \tag{1.23}$$

$$\boldsymbol{x_t = \iint_0^t ((q\left(\frac{v_z B_o x}{a m_p}\right)) dt + v_{x,0}) dt + x_0} \tag{1.24}$$

$$\boldsymbol{y_t = \iint_0^t ((q\left(\frac{v_z B_o y}{a m_p}\right)) dt + v_{y,0}) dt + y_0} \tag{1.25}$$

These equations are the foundation for estimating beam transport through quadrupole lens.

1.2.6 Quadrupole Triplet

A quadrupole triplet was selected as the ion optics because they are ideal for focusing and collimating high-energy particle beams.[3-4] A great benefit to using a quadrupole triplet is that the beam can be focused to a point without astigmatism.[4] A traditional quadrupole triplet consists of three quadrupoles where the first (Q1) and last (Q3) have a length *l* and the middle (Q2) has a length of 2*l*.[4] The distance between them are symmetric and the magnetic field is the same for all three. Our design differs in that all quadrupoles have the same length; this is due to the increased cost of manufacturing "one off" products. However, the same focusing power can be achieved by doubling the magnetic field of the second quadrupole. A schematic of the ion optics design is shown below in Figure 1.5.

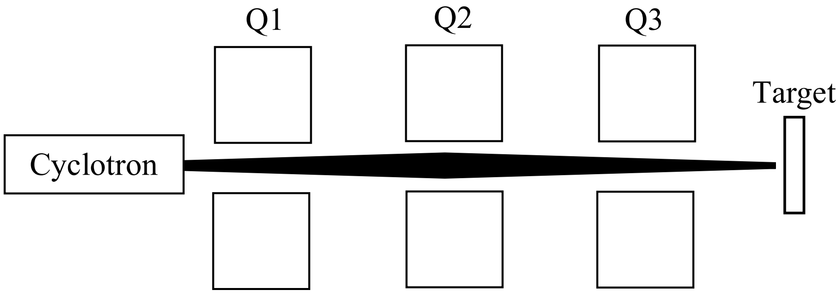

Figure 1.5 A schematic of the ion optical workbench

The ion optic parameters have a large impact on the quadrupole design and simulation. An estimate of the bore size was obtained using the beam divergence, which was calculated in the section above. The bore size was chosen to be large enough to transport the beam and allow for beam focusing, but not be excessively large because the cost of quadrupole magnets increases rapidly as bore size increases. The bore size also directly affects the magnetic field gradient of the quadrupole.

As the bore size increases, the magnetic field gradient decreases. The magnetic field gradient can be increased by increasing the current driven through each coil. However, the current driven through the coils is limited due to heat transfer issues. Air cooled magnets have lower maximum operating currents than water cooled magnets, but water cooled magnets are more expensive. In this work there was a balance between cost and total beam transport.

1.3 GE PETtrace Cyclotron

A schematic of the GE PETtrace cyclotron is shown below in Figure 1.6. H^- ions are extracted out of an ion source in the middle of the cyclotron. A magnetic field confines the negatively charged particles, causing them to fly in a circular path about the center of the cyclotron. An RF electric pulse accelerates the ions, increasing the radius of their circular path larger. Once the particles' orbits are near the exit of the cyclotron, the H^- ions strike a stripping foil. The stripping foil removes two electrons, converting the negative charged particles to protons (H^+); now the charge ***q*** on the ion is +1 causing the force from the magnetic field to be in the opposite direction (see equation 1.3). This causes the H^+ to be pushed out of the cyclotron and into one of the target ports. The stripping foils are precisely moved inside the cyclotron to extract the cyclotron beam out of one of the six target ports. One stripping foil is used for target ports 1-3, and the other is used for target ports 4-6. The beam can actually be extracted out of two ports at the same time, but this technique is not used in this thesis and therefore will not be discussed further. Finally, the current of the beam is monitored at the ion source, stripping foils, targets, and collimators. The collimators are located between the target ports.

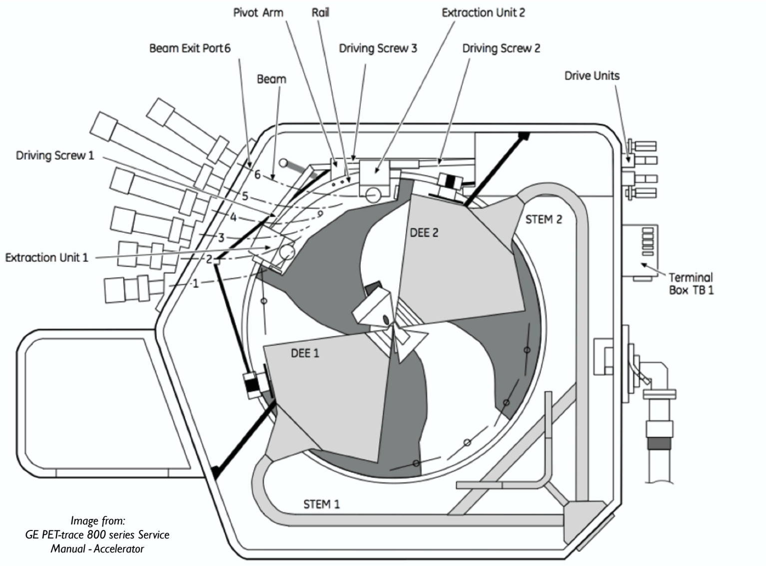

Image from:
GE PET-trace 800 series Service
Manual - Accelerator

Figure 1.6 A schematic of a GE PETtrace cyclotron.[5]

1.4 Brief Description of Thesis Content

This thesis is comprised of 6 chapters what are organized as follows. Chapter 2 explains how SIMION models ion beam transport. It covers the numerical method SIMION uses to estimate the magnetic field strength. It also explains how to make potential arrays and how ion trajectories are simulated. The second half of this chapter reviews, in detail, the design and construction of an industrial beamline for a TR-30 cyclotron. The authors outline how to design and construct a beamline, and provide reasons for their choices. Although the TR-30 is a 15-30 MeV cyclotron many of the topics covered in the papers are directly applicable to a beamline for a GE PET-trace cyclotron. In many ways the papers cover in this chapter can be thought of as design heuristics for high-energy beamlines.

Chapter 3 covers the approach to designing the ion optics, measurement of the cyclotron beam, and design of the ion optics using SIMION. This section details how the cyclotron beam was measured, and the results of the experiments. The SIMION simulations, which were used to find the design parameters of the ion optics, are also discussed. Mapping the magnetic fields of the purchased magnets is also coved in this chapter.

Chapter 4 details the design and construction of the beamline. Included in this is the beamline design, the experimental chamber design, the beam imaging system design, and the instrumentation design. The chapter outlines how the entire system works.

Chapter 5 walks through alignment of the beamline, and discusses characteristics of the transported beam. The characteristics covered include how the stripping foil position effects the beam at the target, how the beam changes with time, and the effect the

HAVAR foils have on the focused beam spot size. The focusing ability of the quadrupole magnets is demonstrated and tabulated as a reference for future users. Finally, in chapter 6, recommended beamline improvements are given.

Chapter 2

Background

2.1 SIMION

2.1.1 Introduction

SIMION 3D version 7.0 (Idaho National Engineering and Environmental Laboratory, Idaho Falls ID) is an ion optics simulation program that models 3D electrostatic and magnetic potential arrays (PAs).[2a] Within the ion optics workbench users can set up and position PAs. The user can also define fly ions (FI) with a specific mass, charge, position, trajectory, and kinetic energy. FIs are simulated ions that are used to visualize how PAs works. User programs can be written within SIMION to accomplish many tasks, such as: varying the kinetic energy of FIs to have a distribution of energies around a specific value, varying the trajectories of FIs to be randomly distributed about a specified cone angle, or scaling the field strength of PAs.

It is important to understand how SIMION models magnetic ion optics to ensure simulations are interpreted accurately. One can easily simulate ion optics in SIMION but that does NOT mean the simulation is accurate. First, I will discuss PAs and how they are constructed, and then I will explain how SIMION uses PAs to model magnetic fields. Finally, I will discuss how SIMION assembles multiple PAs into an ion optics workbench and models ions flying.

2.1.2 Potential Arrays

A 2D view screen shot of the PAs of a quadrupole is shown below in Figure 2.1. The array parameters define how 2D potential arrays are created in the 3D ion optics workbench.

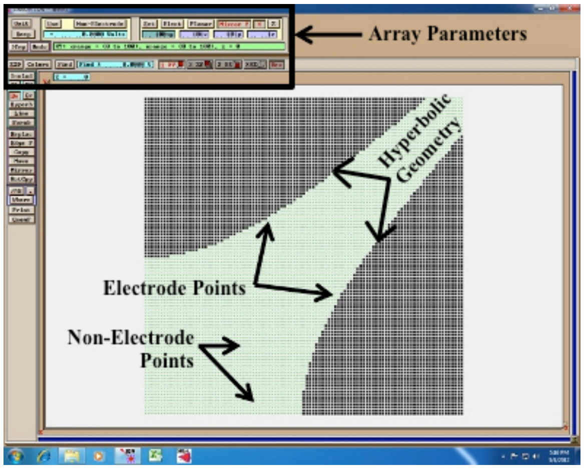

Figure 2.1 Screenshot of 2D geometry of the quadrupole potential array.

The green region (lightly shaded gray when printed in black and white) is comprised of non-electrode points, and the dark region is comprised of electrode points. The two back regions are separate electrodes that can be programed to have different potentials. For magnetic PAs, each electrode is given a “magnetic potential” (Mags). The units of Mags are gauss*grid units; to obtain the magnetic gradient you need to multiply by the number of grid units that separate the electrodes from 0 gauss. For a quadrupole the grid units are from the hyperbolic surface to the center of the quadrupole. In Figure 2.1 the center of the quadrupole is a green dot in the bottom-left-most corner of the non-electrode area. SIMION assumes that magnetic potentials across the electrode surface are constant, which is dangerous to assume because it can lead to inaccurate models.[2a]

A 3D quadrupole PA, shown in Figure 2.1, is generated by setting the array parameters to mirror in both the X and Y plane and assigning the nz value. The nz value is the number of grid units the 2D PA is extrude in the z plane. A 3D PA of a quadrupole with a bore size of 42 mm and a yoke length of 100 mm is shown in Figure 2.2.

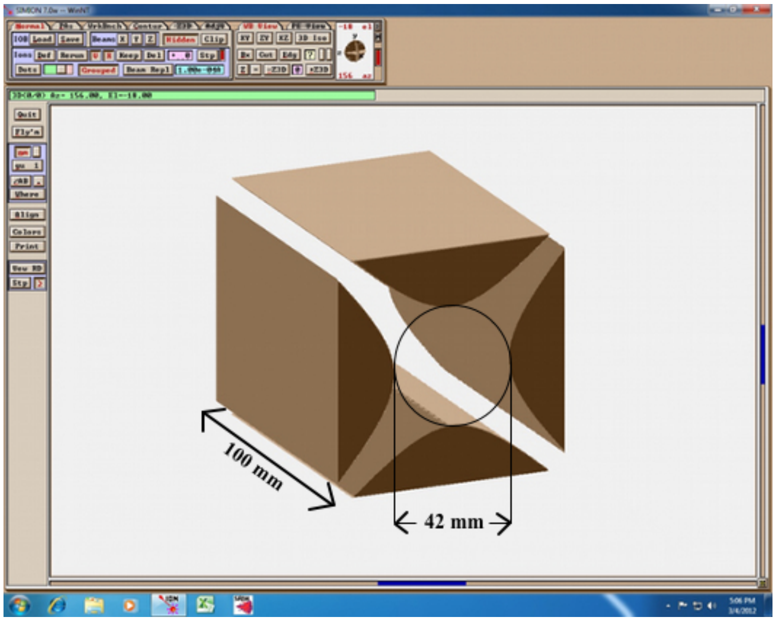

Figure 2.2 Screenshot of a 3D magnetic quadrupole PA in the ion optics workbench.

The program recognizes a PA as a “fast potential array” by assigning a +1 Mags to the bottom electrode and a -1 Mags to the top electrode, see Figure 2.1. This enables users to quickly modify the PA during simulations, see Figure 2.3. In Figure 2.3 the bottom electrode is set to +461.900 using the control bar in the top left, the top electrode has the same magnitude but opposite in sign.

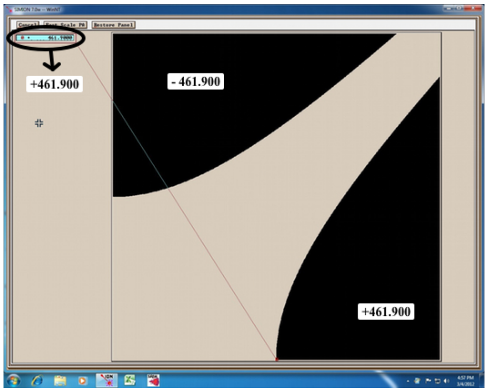

Figure 2.3 ***Screenshot of the quadrupole fast PA scaling menu.***

2.1.3 Potential Arrays Magnetic Field Approximation

SIMION approximates the Laplacian:

$$\nabla^2 \phi_m = 0 \tag{2.1}$$

where ϕ_m is the magnetic potential, by iterating equation 2.2 until the tolerance (equation 2.3) is satisfied. The program uses over-relaxation, a finite difference technique, which minimizes numerical errors and memory usage.[2a] The relaxation method uses the nearest four points, for 2D arrays, (see Figure 2.4) to estimate the electrostatic or static magnetic potential for any point $P0_{new}$ by:

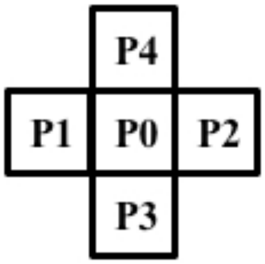

Figure 2.4 ***Diagram of the relaxation method.***[2a]

$$\boldsymbol{P0_{new} = \frac{P1+P2+P3+P4}{4}} \qquad (2.2)$$

$$\boldsymbol{P0_{new} - P0 \leq tolerance} \qquad (2.3)$$

where ***P2***, ***P3***, and ***P4*** are the nearest neighbors of ***P0***. Once the magnetic potential at every point in a PA is estimated, the PA is ready to be used in simulations. Potential energy diagrams can be created to ensure the estimation described above is reasonable.

A potential energy diagram of a quadrupole is shown below in Figure 2.5. The poles on the left and right side shown in black are at the same potential, as they should be because the poles are assigned a specific value. The green lines are what were estimated above, they are smooth and there are no sharp edges; they appear to have accurately estimated the Laplace Equation.

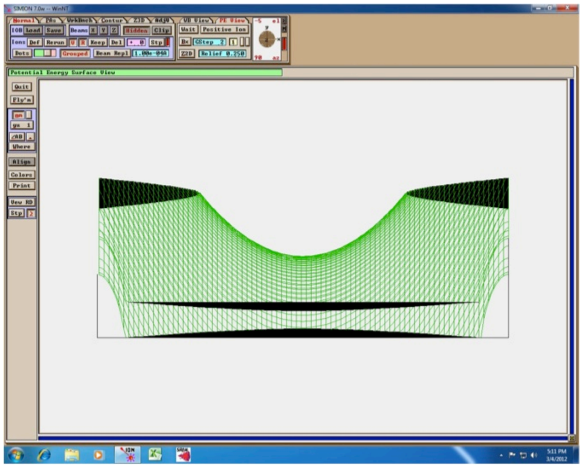

Figure 2.5 SIMION screenshot of a PA potential energy diagram of a quadrupole.

The potential energy diagram above, in Figure 2.5, is also used to help visualize the focusing nature of ion optics in SIMION. Imagine the ion source comes out of the paper, the ion near the top of the "hills" feel more potential than ions near the "valley", and therefore the outermost ions are more strongly focused. This is exactly how a quadrupole should behave and further confirms that a good approximation of the Laplace equation was found.

2.1.4 Ion Optics Workbench

The ion optics workbench is used to simulate the flight of ions as they fly through electrostatic and magnetic fields. Each PA is independently positioned in the workbench. The general workbench setup for all of the simulations is shown below in Figure 2.6. In the workbench, the beam trajectory, the quadrupole PA magnetic potentials, and each PA orientation can be changed. Ions fly out of the ion source and into the quadrupole potential arrays. In the quadrupole PA the ion trajectory is changed due to the magnetic potential it experiences in each quadrupole. If the magnetic potentials are correct the ions are focused onto the target. If the magnetic potentials are wrong, the beam blows up or it does not make it to the target.

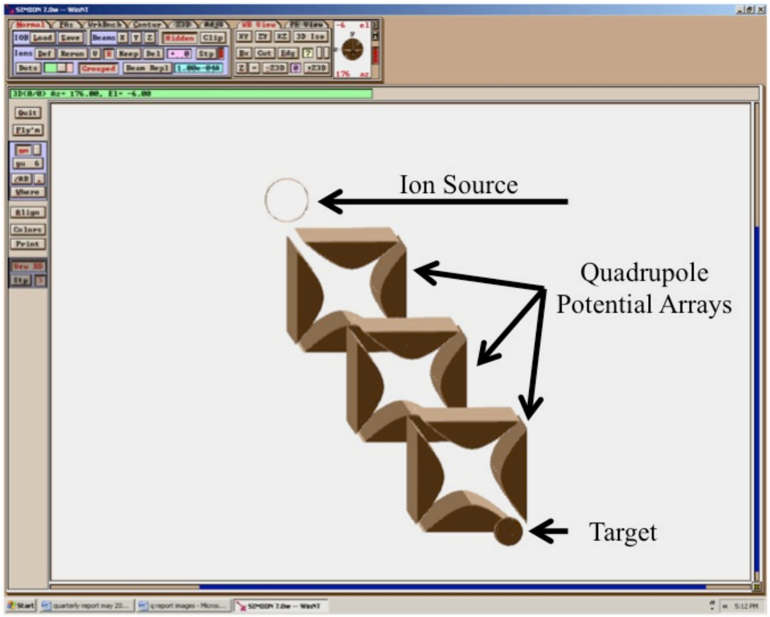

Figure 2.6 SIMION screenshot of the ion optics workbench.

2.1.5 Ion Optics Workbench Approximation

As ion progress through the ion optics workbench they move from one grid unit to the next. Once an ion enters a PA it will experience a force (Figure 2.7).

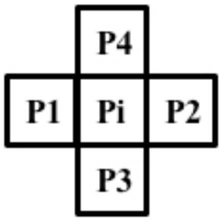

Figure 2.7 Diagram of how the magnetic force an ion experiences in a PA is estimated.[2a]

For a planer 2D magnetic PA, the force an ion experiences is approximated by:

$$\boldsymbol{B_x = ng(P_1 - P_2)} \tag{2.4}$$

$$B_y = ng(P_3 - P_4) \tag{2.5}$$

$$B_z = 0 \tag{2.6}$$

where B_x, B_y, B_z, are the magnetic forces in the x, y, and z direction, respectively. P_n is the magnetic potential (in Mags) at point P_n, and ng is the user adjusted scale factor. The magnetic forces are used to calculate the acceleration (A_x, A_y, A_z) an ion experiences at point Pi by:

$$A_x = \frac{c(v_y B_z - v_z B_y)}{m} \tag{2.7}$$

$$A_y = \frac{c(v_z B_x - v_x B_z)}{m} \tag{2.8}$$

$$A_z = \frac{c(v_x B_y - v_y B_x)}{m} \tag{2.9}$$

where c is the speed light, v_x, v_y, v_z, are the ion's velocity in the workbench, and m is the ion's rest mass divided by it's units charge.

2.1.6 SIMION User Programs

A fly program randomly (see Appendix A) generates 16.5 MeV protons with trajectories within a 3.5 mrad cone angle; a cross-section of the generated beam (37 proton trajectories) entering Q1 is shown in Figure 2.8.

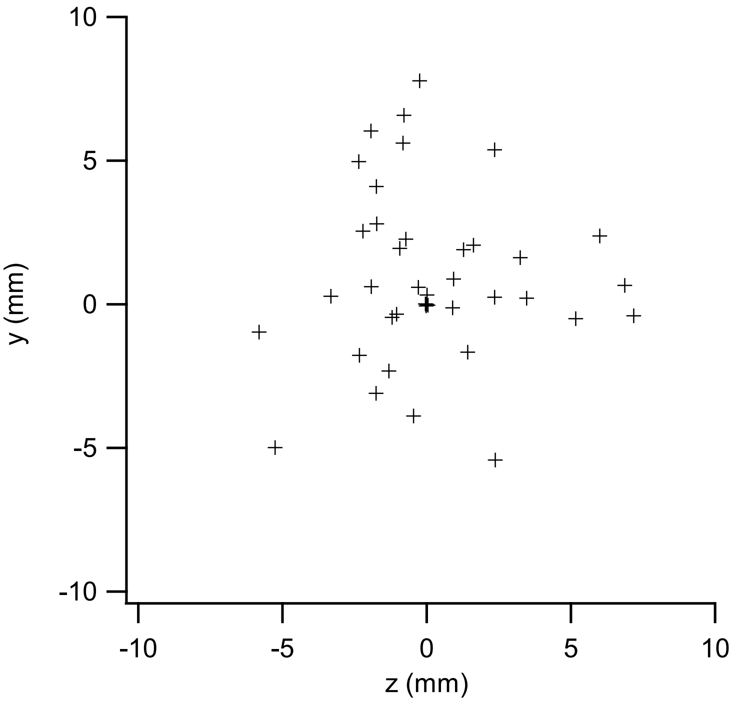

Figure 2.8 Randomly generated ions as they enter the first quadrupole (Q1).

SIMION has no way to calculate fringe fields. A user program was written (Appendix A) that includes the fringe fields generated by the magnets that we purchased.

2.2 Industrial Beamline

2.2.1 Introduction

Industrial beamline design and construction have been outlined[6] in several publications. I will summarize what has been done to paint a complete and clear picture. First, I will cover, in detail, the design of an industrial beamline. Then I will cover beamlines that have been installed on PETtrace size particle accelerators.

2.2.2 TR30 Cyclotron

The TR30 cyclotron (Advanced Cyclotron Systems, British Columbia, Canada, formally Ebco Technologies Inc.) system accelerates H^- ions to an energy range of 15-30 MeV. A schematic of the cyclotron is shown below in Figure 2.9.

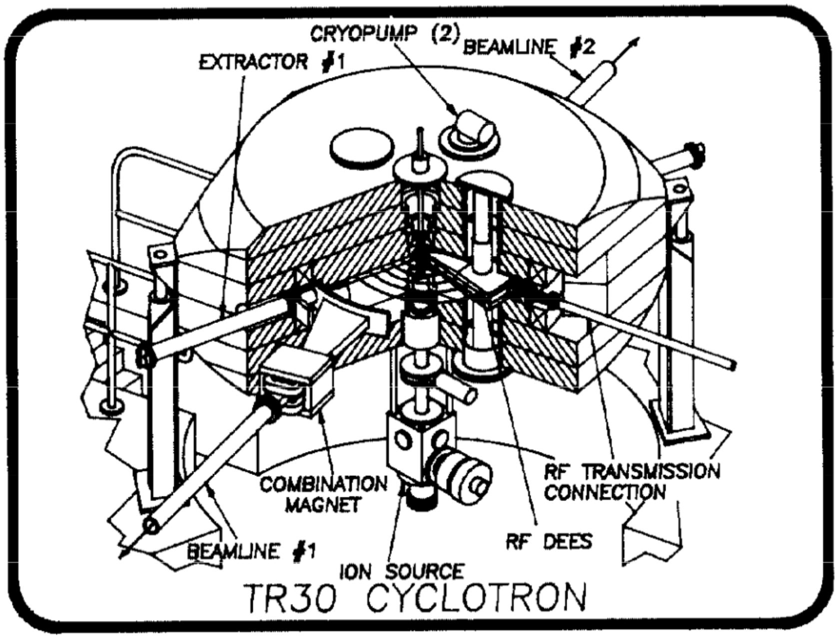

Figure 2.9 Schematic of the TR30 Cyclotron[7]

An external ion source injects H^- ion into the center of the cyclotron. The cyclotron is a four-sector compact design with radial ridge hills, and RF dees accelerate the ion beam.[7] The radial ridge hills provide beam focusing while the beam is accelerated. Ions are contained and accelerated in the horizontal plane. The cyclotron parameters are shown below in Table 2.1. Two independent stripping foils can extract the beam simultaneously; each foil can extract beam currents up to 250 uA at 15 MeV and 225 uA at 30 MeV.[7]

Table 2.1 The TR30 cyclotron parameters[7]

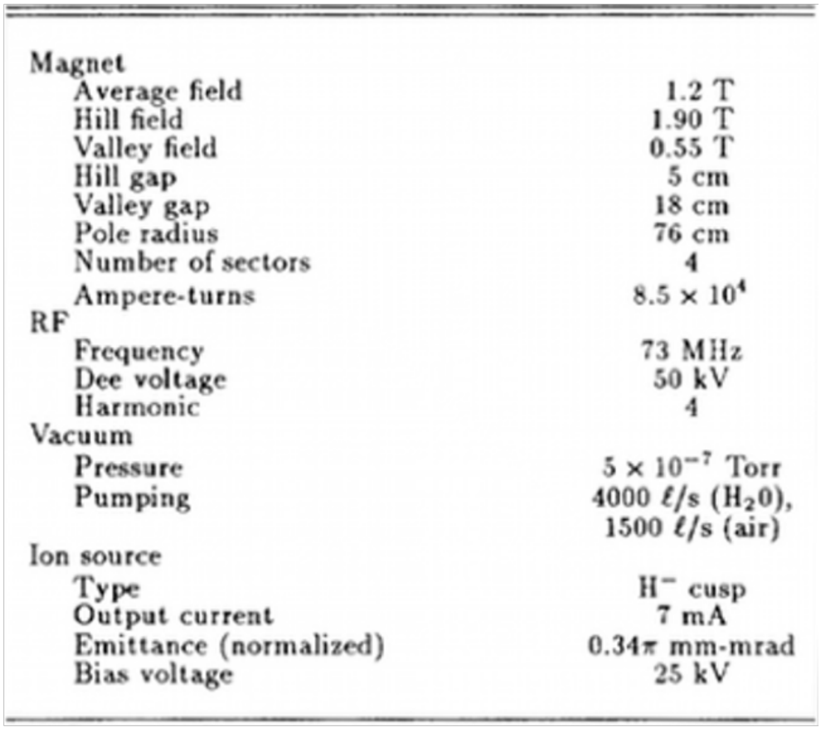

Magnet	
Average field	1.2 T
Hill field	1.90 T
Valley field	0.55 T
Hill gap	5 cm
Valley gap	18 cm
Pole radius	76 cm
Number of sectors	4
Ampere-turns	8.5×10^4
RF	
Frequency	73 MHz
Dee voltage	50 kV
Harmonic	4
Vacuum	
Pressure	5×10^{-7} Torr
Pumping	4000 ℓ/s (H_20), 1500 ℓ/s (air)
Ion source	
Type	H^- cusp
Output current	7 mA
Emittance (normalized)	0.34π mm-mrad
Bias voltage	25 kV

2.2.3 Industrial Beamlines

M. P. Dehnel et al. first outlined[6c] the design and operation of an industrial beamline in 1991. Custom beamlines were made for specific experimental purposes but they give the foundation to properly design a beamline; you can think of this paper as beamline design heuristics.

2.2.4 Industrial Beamline Design Considerations

First they established beamline optical constraints, see Table 2.2. The constraints imposed were due were due to safety, power availability, the size of the vault, and finally the needs of the user. The beamline, ion optics, and diagnostics were all designed to work within the defined constraints.

Table 2.2 Beamline Optical Constraints[6c]

Description	Value	Imposed By
Particle Type	Proton	User
Particle Energy	15 to 30 MeV	User
Cycltron to Primary	1° Left at 30 MeV	Safety & Power
Beamline Bend	15° Left at 15 MeV	Safety & Power
Number of Secondary Beamlines	3	User
Secondary Beamline Bend Angles	12.5° Left	User
	12.5° Right	User
	1° Right	User
Spot Size on Target		User
Horizontal	1 cm	User
Vertical	2.4 cm	User
Cyclotron to Secondary Beamline Length	3.88 m	User
Secondary Beamline Length	3-5 m	Vault Wall Thickness
Input Proton Beam at Stripper Foil	at 30 MeV	Ebco TR30 Cyclotron
Horzontal Width	0.0075 cm	Ebco TR30 Cyclotron
Horizontal Divergence	2.910 mrad	Ebco TR30 Cyclotron
Vertical Width	0.16 cm	Ebco TR30 Cyclotron
Vertical Divergence	2 mrad	Ebco TR30 Cyclotron
Momentum Spread	0.370%	Ebco TR30 Cyclotron
Permissible Beam Spill	<10%	User

2.2.5 Beamline and Ion Optics Design

A diagram of the industrial beamline is shown below in Figure 2.10. Charged particle optics code was used to design the magnets.[6c] The beamline bore is 95 mm ID and approximately 8 m long.[6c] The maximum half-width beam envelope is approximately 2 cm.[6c] Aluminum components were used wherever possible to limit the amount of residual activity.[6c] They used cryopumps rather than diffusion pumps because it limits the chance of oil contaminating the vacuum system.[6c]

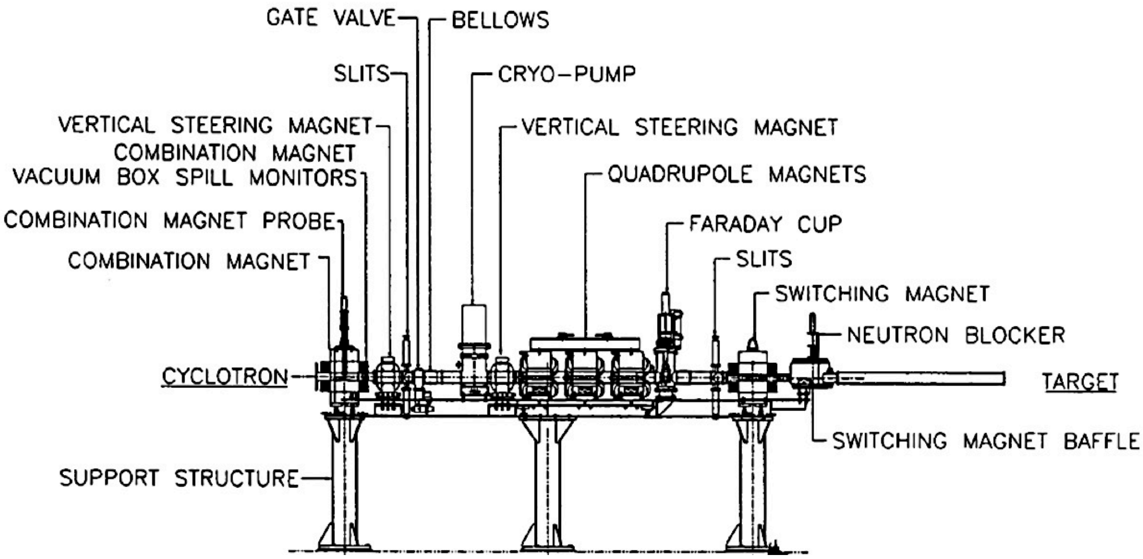

Figure 2.10 Physical layout of an industrial beamline.[6c]

A 15-30 MeV proton beam is extracted out of the cyclotron by adjusting the stripper foil that resides inside the cyclotron.[6c] The beam energy, and horizontal angle changes due to the stripper foil position.[6c] The combination magnet corrects the beam variation caused by the stripper foil position and centers the proton beam on the horizontal centerline.[6c] This is done by varying the magnetic field strength of the combination magnet to compensate for the beam angle created due to beam extraction at the stripper foil.[6c]

A set of vertical steering magnets centers the proton beam in the vertical centerline.[6c] The first vertical steering magnetic field is adjusted until the beam intersects the vertical centerline at the second vertical steering magnet.[6c] The magnetic field of the second steering magnet is adjusted until the beam is centered vertically down the beamline.[6c] The vertical beam trajectory is relatively stable, and therefore requires relatively low magnetic fields to correct any vertical misalignment.[6c]

A quadrupole triplet is used to focus the beam down the primary beamline.[6c] Vertical and horizontal alignment is needed to keep the quadrupoles from steering the beam.[6c] A quadrupole triplet was chosen over a quadrupole doublet. A triplet allows for focusing of both planes to a single point, where as a doublet focuses each plane to different points.[6c] The triplet also transports the beam with a smaller beam envelope.[6c] Finally, dipole magnet at the end of the primary beamline is used to position the focused beam into one of the three secondary beamlines.[6c]

2.2.6 Design Materials and Considerations

The industrial beamline was designed to limit the amount of radiation workers receive.[6c] This was accomplished by designing a beamline that could be assembled, aligned, and maintained quickly.[6c] Also, materials that activated less than other were used, when possible, to reduce the overall radiation fields.[6c] Finally, the magnets and beamline were designed to transport a majority of the beam and to reduce the amount of beam striking the sidewall of the beamline. [6c] Below in Table 2.2 are the design material considerations that were used to design of the industrial beamline.

Table 2.3 Design material considerations used[6c] by the authors

Radiation resistant electrical insulation materials
Polyimide
Machinable ceramic
Ceramic stand-offs
Anodized aluminum
Low activation materials
Graphite
Aluminum
Radiation resistant wires
Polyimide coated wires
nonpolyamide based cabling
Radiation resistant and electrically insulated water tubing
Polyurethane tubing
Radiation resistant sub-components
Methamine terminal blocks
steel tie wrap (as opposed to polyamide)
air cylinders with radiation resistant seals
Quick release equipment
Quick disconnect vacuum flanges for all devices to avoid bolt-on flanges
Quick disconnect bayonet of BNC connectors for control cabling
Quick release water fittings with no polyamide permitted

2.2.7 Beam Diagnostics

The authors use a variety of diagnostics to monitor the beam throughout the beamline. The design and function of each diagnostic will be discussed to introduce you to various techniques. A combination magnet probe was used to intercept the whole beam during low current tuning.[6c] The probe is a water-cooled graphite finger that actuates in and out of the beamline. This probe is used when the magnets are off to ensure the beam trajectory is properly entering the first bending magnet; the probe is removed from the beamline once the current is maximized.[6c]

The combination magnet vacuum box spill monitors are made of stationary water-cooled graphite blocks. One block on the left and one block on the right skim the sides of the beam and can therefore be used to determine the trajectory after the combination magnet.[6c]

The Slits diagnostic is only 100 mm long and consist of 4 independently adjustable water-cooled graphite beam blockers.[6c] The slits are used for general beam alignment, and can be positioned almost anywhere along the beamline due to it's small footprint.[6c]

A faraday cup can be actuated in and out of the beamline.[6c] The faraday cup consists of a water-cooled graphite-lined cup that accurately measures the total beam current.[6c] The cup was designed to capture all secondary emission electrons created by the beam striking the cup.[6c] The faraday cup is used during low current operation to tune the beam and used as a beam dump during upstream tuning.[6c] The faraday cup is also used as a beam stop when the beamline to "off"; this allows workers to safely service the downstream beamline while the cyclotron sends a beam down other beamlines.[6c]

A switching magnet baffle is located directly after the switching magnet.[6c] The aluminum baffle consist of three graphite coated ports and is water cooled.[6c] The beam current that strikes the baffle is monitored and is used to determine if the beam is aligned down the one of the three secondary ports.[6c]

When the beamline is in the off position, neutrons still travel through the graphite faraday cup. To protect workers, they designed a neutron blocker which is lowered into the beamline.[6c] The neutron blocker is simply a chunk of borated polyethylene.[6c]

2.2.8 Beamline Operation

The authors created a beamline control system, which consisted of two layers. The first layer interfaced devices, operated the devices, and handled the safety interlocks.[6c] The second layer was a software interface that allowed for operation of the beamline by a computer.[6c] The user program was capable of data monitoring, data logging, alarming, and automated control.[6c] They outline a normal procedure for operating the beamline; the procedure is shown below in Table 2.4. The authors point out that only recently (paper published in 1991) have beamlines become automated, and before then, the operators where required to complete many of the feedback loops necessary to maintain beam on target.[6c]

Table 2.4 The normal procedure for beamline operation.[6c]

1) The cyclotron, targets, and vacuum are set up automatically ahead of time by the control system.
2) From the main menu, the beamline page is selected.

3) Beamline settings (magnetic field settings) appropriate for the production run are retrieved and assigned to the beamline magnets.
4) Automatic extraction of beam from the cyclotron is initiated if interlocks are satisfied.
    a) Beam proceeds to target at low current (it may only go to the Faraday cup if a new tune is being worked on).
    b) Beam current is ramped up to operating level (usually about 200 uA)

    c) Magnet field settings are automatically adjusted according to spilled beam current readbacks from diagnostic devices.
    d) During run time, the beam spill is automatically minimized along the beamline to < 5% (usually) by the control system.
5) The operator can intercede to set magnetic fields from the command line if he/she so desires.
6) If the beam spill on any diagnostic device is over 10 uA, the device control layer will switch the beam off.

Chapter 3

Cyclotron Beam Estimation & Ion Optics Design

3.1 Design Approach

3.1.1 Introduction

The block flow diagram below shows the iterative process undergone to design the ion optics (see Figure 3.1). The literature review was used to find a quick and accurate method for measuring the cyclotron beam. Once the cyclotron beam profile was determined the ion optics were designed. A literature review was also used to determine what ion optics should be considered; a quadrupole triplet was found to be the ideal ion optic. SIMION, a finite element software package, was used to design the ion optics once the cyclotron beam profile was known.

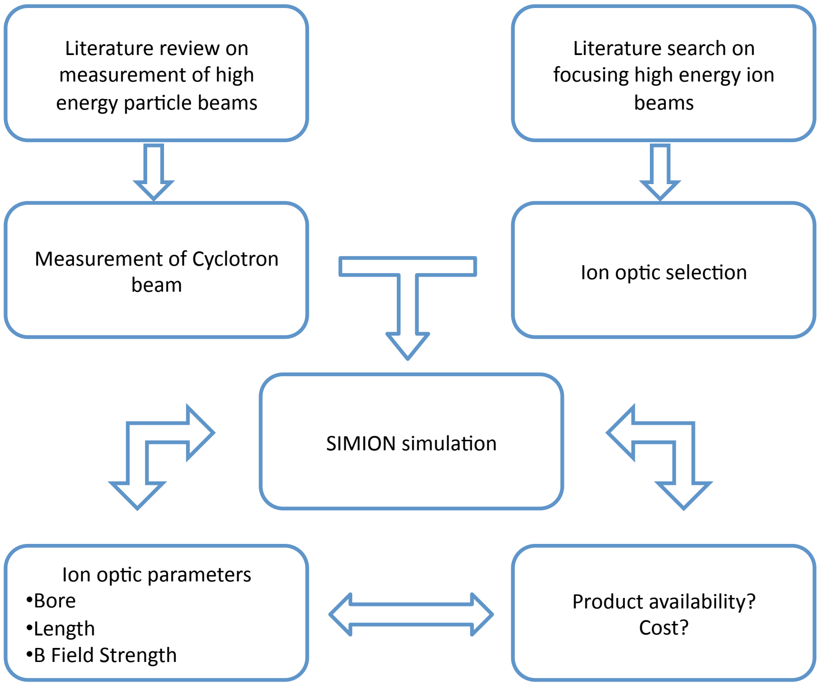

Figure 3.1 A block flow diagram of the ion optic design process.

3.2 MURR Cyclotron Beam Estimation

3.2.1 Introduction

To size the ion optics, a good estimation of the cyclotron beam position and beam divergence was needed. This was accomplished by taking beam images at two different distances from the cyclotron. Images of the beam were obtained using a technique described[1] by Avila-Rodriguez; a metal foil or plate secured to the end of the beamline and activated with the proton beam. Following irradiation self-developing radiochromic film is exposed to the plate surface. The film changes color due to dose; this color change is used to generate the beam image. The beam trajectory was found by drawing a line through the maximum intensity of the beam images. The beam divergence was estimated by comparing full width half max of the two images. The beam position and beam distribution can be calculated any distance from the cyclotron by knowing the initial position and divergence of the beam.

3.2.2 Background

Radiographic film was selected as the beam measurement technique for several reasons. The film is very cheap (1000x) relative to ion beam profilers. Radiographic film is readily available and no specialized equipment is needed to process the film. This enables the experiments and data processing to be completed quickly. Gafchromic EBT2 film (International Specialty Products, Wayne, NJ, USA) is a self-developing film that changes color under irradiation. The film undergoes a polymerization reaction upon exposure to ionizing radiation; this causes a color change in the active layer. Gafchromic EBT2 film is capable of measuring up to 40Gy using the green color channel.[8] The optical density of the film can change as much as 8% after irradiation.[9] Cheung et al. showed that 24 hours after exposure the polymerization reaction stabilizes.[10] The film is documented[9, 11] to have little energy dependence. Although inspection of the film with the naked eye reveals the beam position, it has been demonstrated[1] that image processing can reveal beam distribution.

3.2.3 Radiochromic Film Calibration

Gafchromic EBT2 dosimetry film samples were irradiated by a Cs-137 source. The samples were irradiated for different lengths of time to generate a color response to dose. The polymerization reaction was allowed to approach steady state before the film was scanned; this was accomplished by waiting at least 24 hour prior to scanning the film samples. The samples were scanned using an Epson Perfection V500 Photo scanner and Image J (National Institute of Health), an image processing software package, was used for image processing. Image processing consisted of isolating the red color channel and finding the mode pixel intensity. The mode pixel intensity value was set equal to the dose the film sample received. A fourth order polynomial fit was used to correlate pixel value to dose, see Figure 3.5.

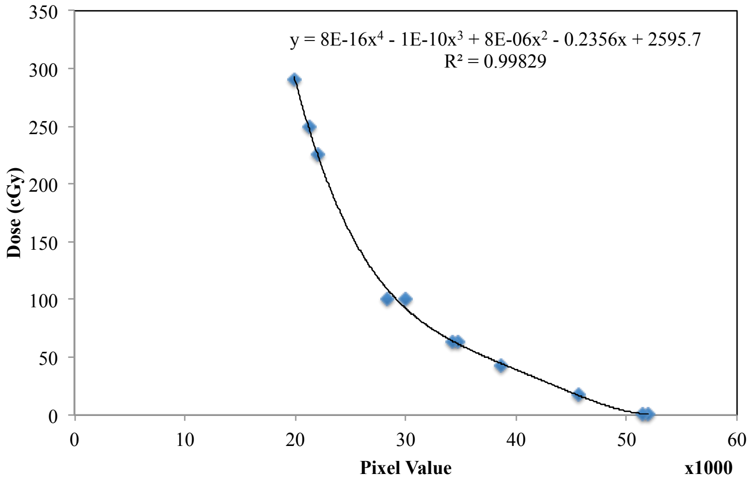

Figure 3.2 Radiographic film calibration using a Cs-137 dose equivalent source.

3.2.4 Beam Estimation Experimental Method

These measurements were conducted using existing equipment to reduce the time spent designing the ion optics and to minimize cost. Two target holders (see Figure 3.3), served as points to measure the beam.

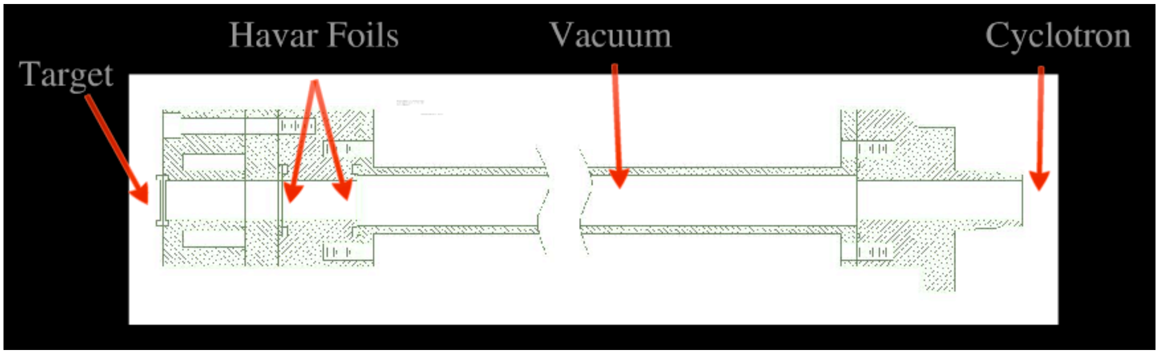

Figure 3.3 A diagram of the target holder used to measure the cyclotron beam characteristics.

The beam was extracted at the 2nd target port of the cyclotron. The extracted beam travels down an evacuated drift tube, penetrates two HAVAR foils, and then strikes the target. The HAVAR foils act as a physical barrier between the cyclotron and the target. Helium can be pump between the HAVAR foils for cooling; No He was pumped due to the low currents and short irradiation periods. Drift tubes 19.3 cm and 56.8 cm in length were mounted to the cyclotron. A 0.25 inch thick copper plate placed at the target was irradiated at 10-12 uA for one minute. After irradiation, radiographic film was exposed to the surface of the copper plate until a substantial color change was observed. The film was then scanned and Image J was used to process the images.

3.2.5 Beam Estimation Results and Discussion

The beam profile for the short and long drift tubes can be seen in Figure 3.4 and Figure 3.5, respectively. The beam is elliptical and the intensity drops quickly away from the peak. The intensity of the beam was estimated by integration of the dose over the beam area. Full width half max of the beam, 56.8 cm from the cyclotron, was estimated to include 52% of the total beam and have a 14 mm diameter with a 3.5 mrad divergence. The HAVAR foils and air between them altered the beam but we use this data as a “worst case scenario” for designing our ion optics.

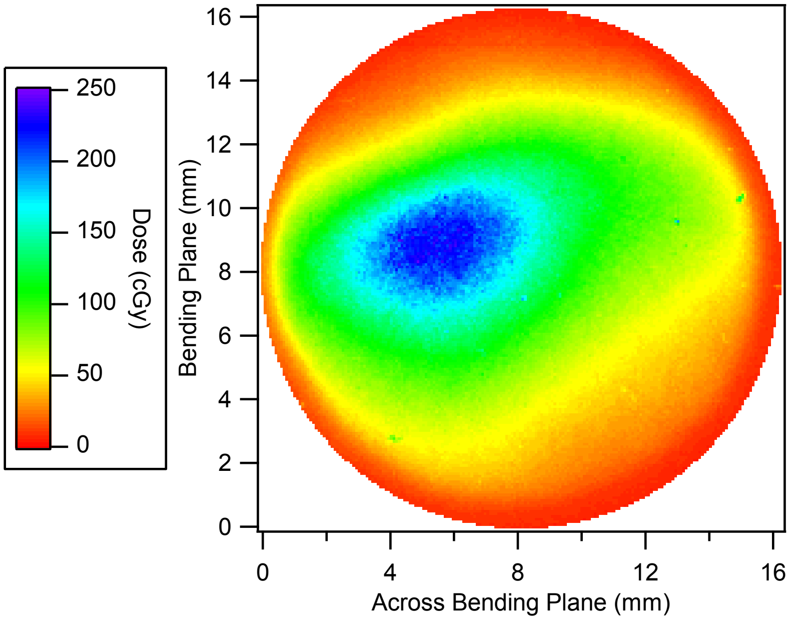

Figure 3.4 Proton beam profile & distribution 19.3cm from the cyclotron exit.

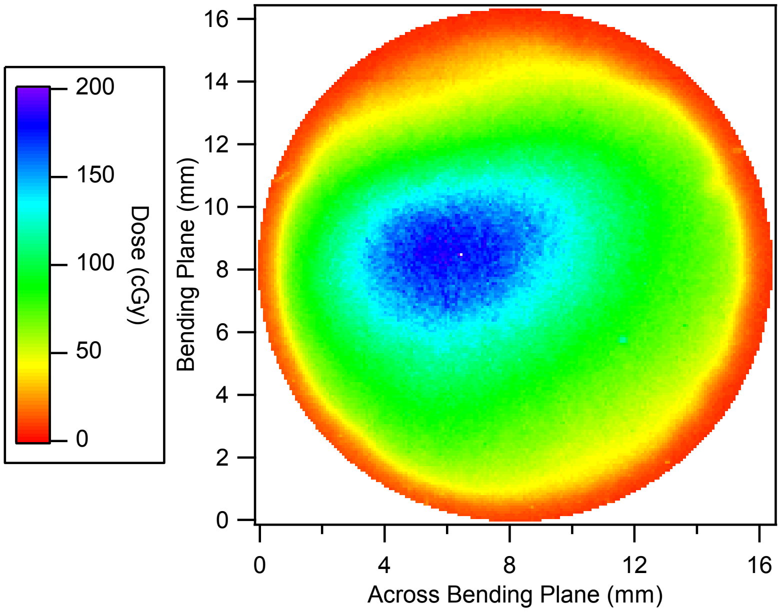

Figure 3.5 Proton beam profile & distribution 56.8cm from the cyclotron exit.

3.3 Ion Optic Design

3.3.1 Introduction

SIMION (FEM software) was paramount in the design of the ion optics. Three sets of simulations were conducted: base case simulations, design simulations, and refined simulations. The fixed and variable inputs used in all the simulations are shown below in Table 3.1.

Table 3.1 The fixed and variable inputs used in the SIMION simulations.

Description	Base Case	Design	Refined
Beam input			
Particle type	Proton	Proton	Proton
Energy	16.5 MeV	16.5 MeV	16.5 MeV
Diameter	14 mm	14 mm	14 mm
Divergence	0	0-3.5 mrad	0-3.5 mrad
Energy spread	0	0-2%	0-2%
Quadrupole PA			
Bore Size	Variable	Variable	42 cm
Yoke length	Variable	Variable	10 cm
Magnetic field strength	Variable	Variable	Variable
Workbench			
Q1 position	> 1.2 m from the cyclotron	> 1.2 m from the cyclotron	> 1.2 m from the cyclotron
Distance between Q1, Q2, & Q3	Variable	Variable	Variable

The base case simulations were conducted using a laminar beam approximation, which is recommended[4] by Humphries; these simulations determined the approximate magnetic field strength needed to focus the proton beam. Design simulations were conducted using the beam estimated in section 3.2. These simulations determined the bore diameter, yoke length, magnetic field strength, and rough position of Q1, Q2, and Q3.

Then venders were contacted to find products that matched the design simulations. Finally, refined simulations were conducted with a user program that included the fringe magnetic fields of the purchased quadrupoles. These simulations provided final position and magnetic field strength needed to focus the proton beam.

3.3.2 Base Case Simulation Experimental Setup

The setup of quadrupole PA was covered in section 2.1. The workbench setup for the base case simulations is shown below in Figure 3.6.

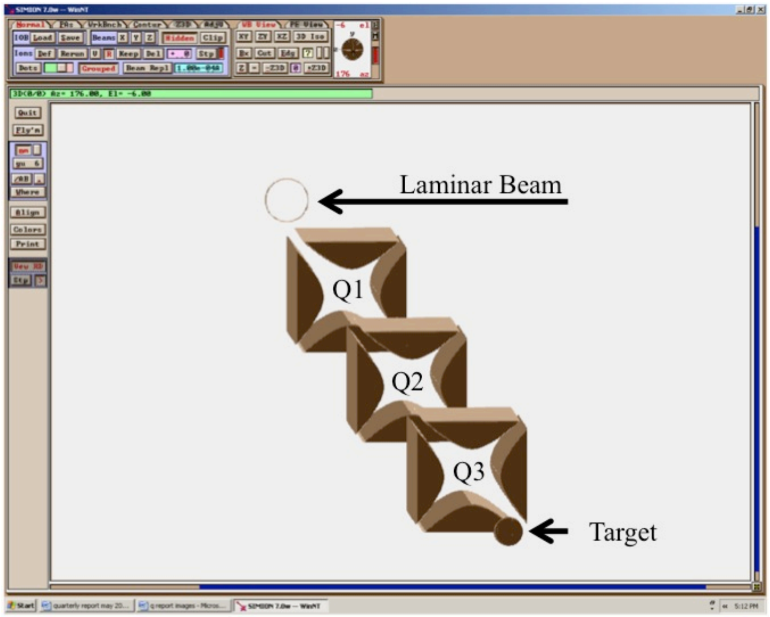

Figure 3.6 Workbench setup of the base case simulations.

Q1 was positioned 1.2 m from the laminar beam source. The bore size and yoke length of the quadrupole potential arrays were adjusted during the simulations to allow for 100% of the beam to be transported through them. The magnetic field strength and distance between Q1, Q2, and Q3 was varied until a tightly focused spot was achieved.

3.3.3 Design Simulations Experimental Setup

The input parameters and workbench setup for the design simulations are shown above in Table 3.1 and Figure 3.6, respectively. The real cyclotron beam was used instead of a laminar beam. The magnetic field strength and distance between Q1, Q2, and Q3 was varied until a tightly focused spot was achieved.

3.3.4 Refined Simulations Experimental Setup

The input parameters and workbench setup for the refined simulations are shown above in Table 3.1 and Figure 3.6, respectively. The real cyclotron beam was used instead of a laminar beam. The bore size and yoke length of the purchased magnets were used, and the fringe fields were added to the simulation code. The magnetic field strength, the distance between Q1, Q2, and Q3, and the target position was varied until a tightly focused spot was achieved.

3.3.5 SIMION Simulations Discussions & Results

SIMION was used to determine the quadrupole specification for manufacturing, and was also used to estimate the installation position of each quadrupole in the cyclotron vault. A plot of a design simulation can be seen in Figure 3.7. The energy spread of the beam was set to 0 for this simulation. Other arrangements of the magnets position will also focus the beam but the magnetic field gradient and target position will change. The ions focus differently in the two planes due to the nature of quadrupoles.

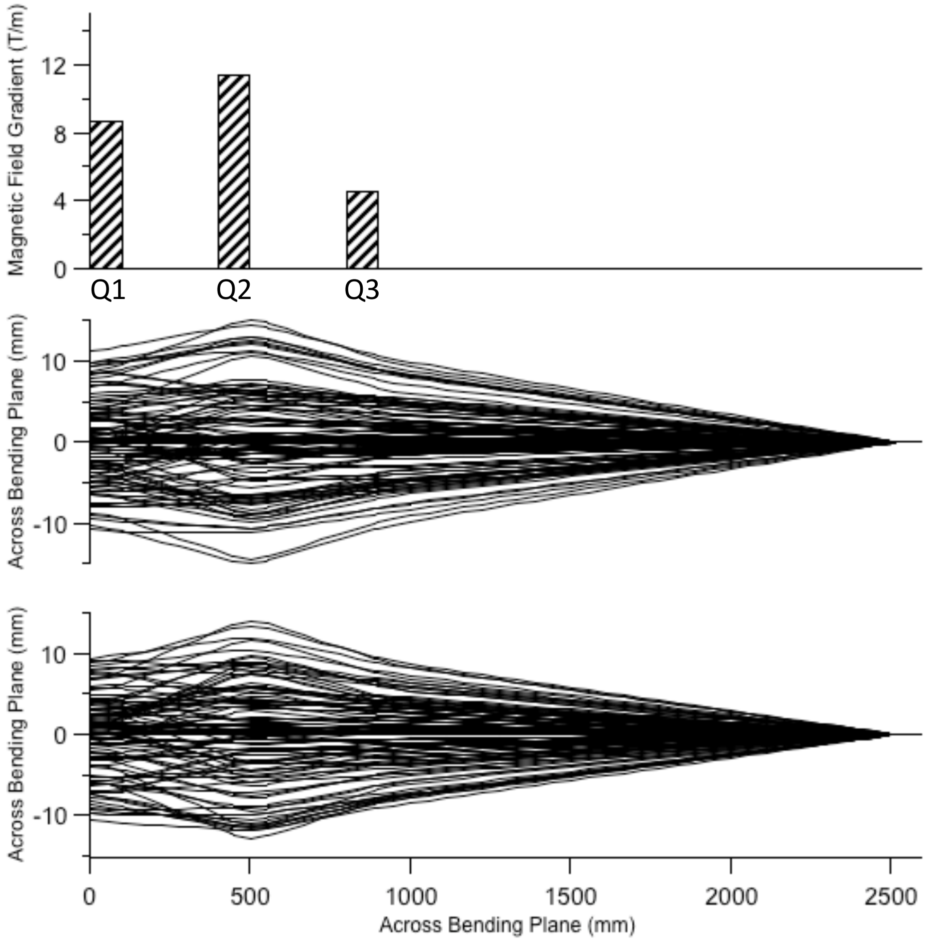

Figure 3.7 Top: The magnetic field the SIMION simulation. Middle: A plot of the beam position across the bending plane of the cyclotron magnet. Bottom: A plot of the beam position in the bending plane of the cyclotron magnet.

The ions converge on the target approximately 3.7 m from the cyclotron; a cross section of the target is shown in Figure 3.8. The SIMION simulation can focus ions to a spot size of about 10 um in diameter. However, it is important to remember that this is only a simulation and the actual beam size will be larger due to the natural energy spread of the beam.

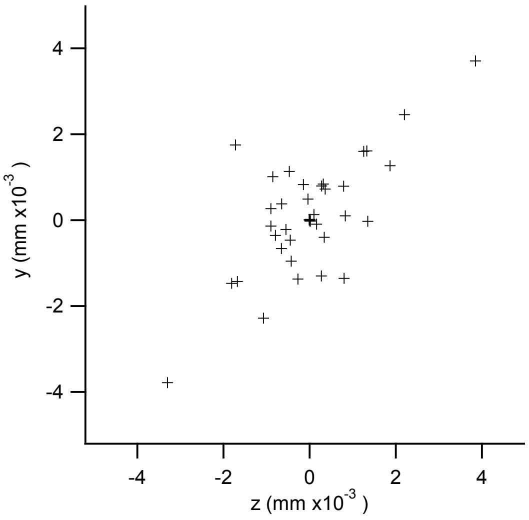

Figure 3.8 A cross section of the target.

A disadvantage of SIMION is the potential arrays are either ON or OFF. There is no decrease in magnetic field outside a potential array. An example of a real magnetic field profile is shown in Figure 3.10 and due to the limitations of SIMION a 10 cm PA was used in the design simulations and the fringe fields were initially ignored. The SIMION potential arrays were only 10 cm long due to the sharp decrease in field strength beyond 10 cm. The vender's hyperbolic surface geometry is slightly different than what was simulated but was assumed to be close enough for design purposes.

Refined simulations included the fringe fields, and the simulations determined that the fringe fields simply decreased the magnetic field strength needed to focus the beam.

3.4 Purchased Quadrupole Magnets

3.4.1 Purchased Quadrupole Magnets

Venders provided design specifications for their quadrupoles. The specifications included: bore size, yoke length, and maximum operational magnetic field gradient. Base case simulations found that the quadrupoles sold by Radiabeam Technology could focus the proton beam. A cad drawing and the design specifications of the quadrupole magnets are shown below in Figure 3.9 and Table 3.2.

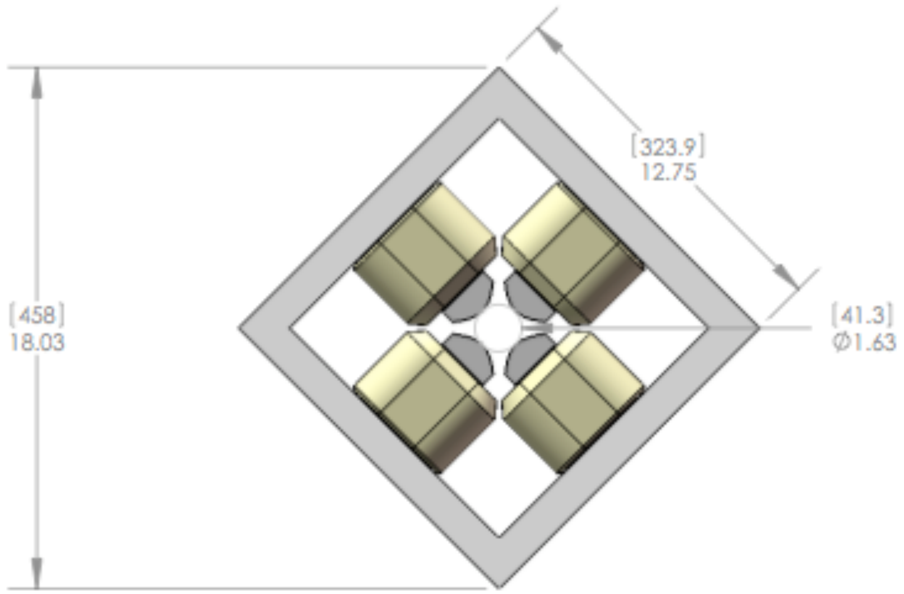

Figure 3.9 Cad drawing of the quadrupole magnets provided by Radiabeam.

Table 3.2 Properties of quadrupole magnets provided by Radiabeam.

Physical Properties		Units
Estimated Weight	36.6	Kg
Material	1006-1010	
Yoke Dimensions (H x W x L)	18.75 x 18.75 x 3.94	Inches
Max. Physical Length	6.3	Inches
(including coils)		
# of coil turns	251	
Calc. Electrical Properties		
Current	9.2	Amps
Current Density	1.4	Amps/mm^2
Voltage per coil/quad	3.25/13	Volts
Resistance per coil/quad	.35/1.2	Ohms
Power per coil/quad	29.8 / 119	Watts
Magnetic Properties		
Magnetic Length	~150	mm
Gradient	12.8	T/m
Integrated Grad	1.9	T

The bore size is large enough to transport a large portion of the beam. The bore size is also small enough that the operating current needed to focus a 16.5 MeV proton beam is low enough that the magnets can be air-cooled. A plot of the magnetic field gradient provided by the vendor is shown below in Figure 3.10.

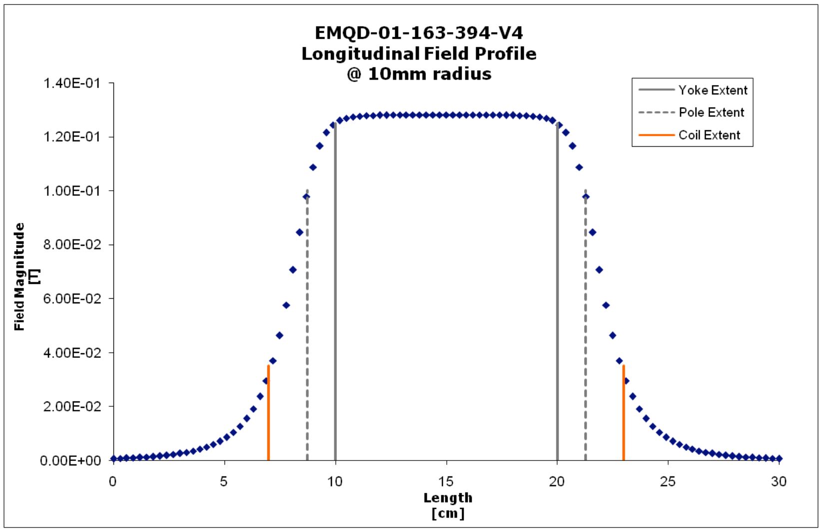

Figure 3.10 Magnetic field profile of purchased magnets provided by Radiabeam Technology.

3.4.2 Experimental

The fringing fields of each quadrupole magnet were estimated using a hall probe; an image of the experimental setup is shown below in Figure 3.11.

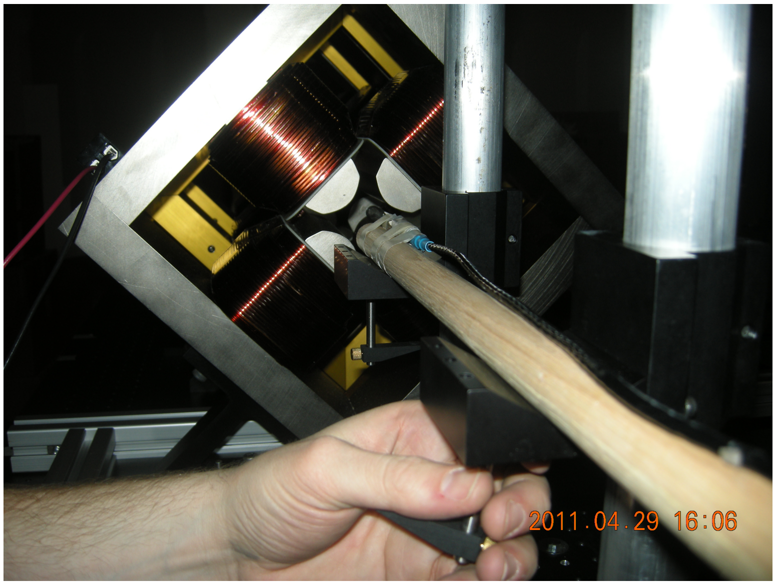

Figure 3.11 The experimental setup used to map the magnetic field of the quadrupoles.

The magnets were secured to the breadboard table and two mounts were positioned parallel to the quadrupole yokes. A 1.067 V potential was applied across each quadrupole (1.1-1.3 ohm resistance) to drive approximately 1 A current. The maximum value of the hall probe was reached if the current was increased above 1 A. The hall probe, tapped to a wooden dowel rod, was incrementally slid through each quadrupole, and the magnetic field was recorded every 0.5 inches. At each increment, the hall probe was rotated until the maximum magnetic field was found. A total of 19 data points were taken for each magnet.

3.4.3 Results and Discussion

Only one set of data was collected for each quadrupole. The magnetic field of each quadrupole, compared to quadrupole data provided by Radiabeam is shown in Figure 3.12. The measured data compares well with the data provided by Radiabeam.

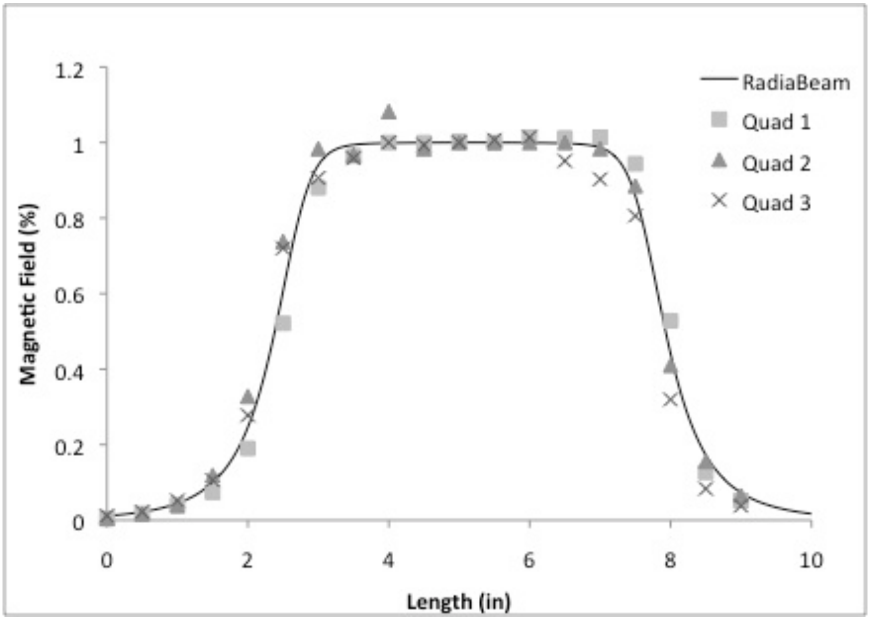

Figure 3.12 Measured magnetic field of each quadrupole compared to data provided by Radiabeam Technologies.

Chapter 4

Design and Construction

4.1 Design and Construction

4.1.1 Introduction

A schematic of the beamline is shown below in Figure 4.1. A list of the beamline components is shown below in Table 4.1.

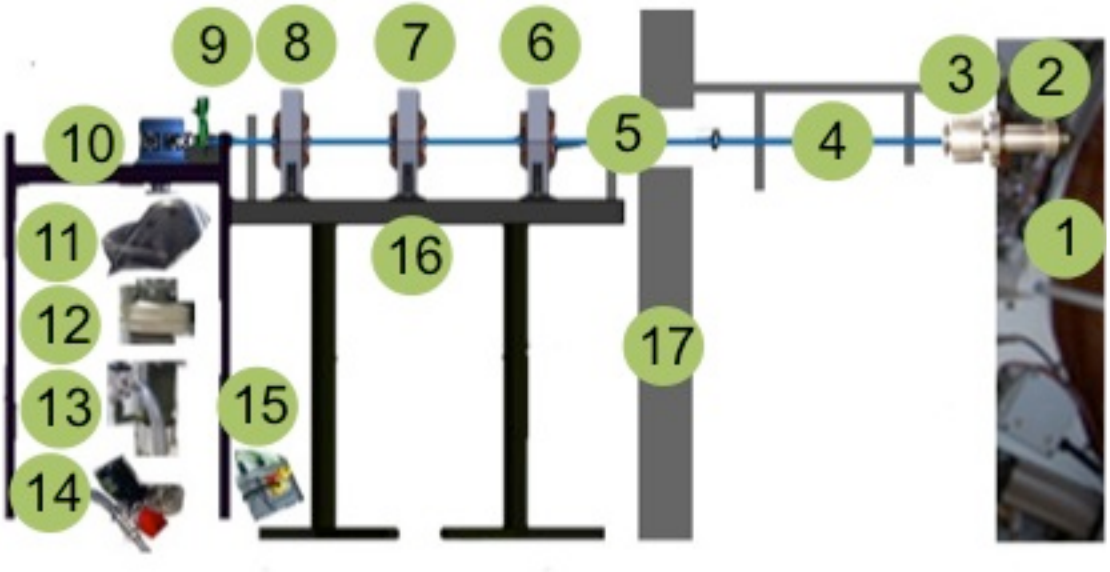

Figure 4.1 A schematic of the beamline

Table 4.1 A list of the beamline components

Component	Tag #
cyclotron	1
KF40 cyclotron adapter	2
collimator	3
short drift tube	4
long drift tube	5
quadrupole #1	6
quadrupole #2	7
quadrupole #3	8
VAT Valve	9
vacuum chamber and table	10
gate valve	11
liquid nitrogen baffle	12
oil diffusion pump	13
mechanical pump	14
solid-state relay box	15
breadboard table	16
concrete wall	17

4.1.2 Beamline

The proton/deuteron beam is extracted from the 2nd target port of the Cyclotron. The adaptor, shown in Figure 4.2, enables a KF 40 flange to connect directly to the cyclotron beam port.

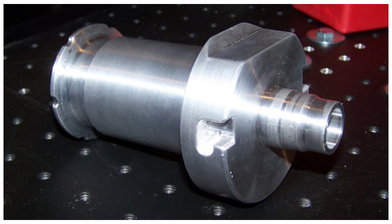

Figure 4.2 An image of the cyclotron adapter flange.

A vacuum break composed of two HAVAR foils (each 20um thick), cooled with helium, isolates the cyclotron from the irradiation platform. Two aluminum tubes (1.12 inches ID

1.25 inches OD) 42 inches and 90 inches long transport the beam through the ion optics to the experimental chamber. The VAT mini gat valve shown in Figure 4.3 is located between the beamline and the experimental chamber, isolates the experimental chamber from the beamline. This valve allows the experimental chamber to break vacuum without breaking vacuum on the entire beamline.

Figure 4.3 An image of the VAT mini valve.

4.1.3 Experimental Chamber

An image of the assembled experimental chamber with vacuum system and diagnostics is shown below in Figure 4.4 Left.

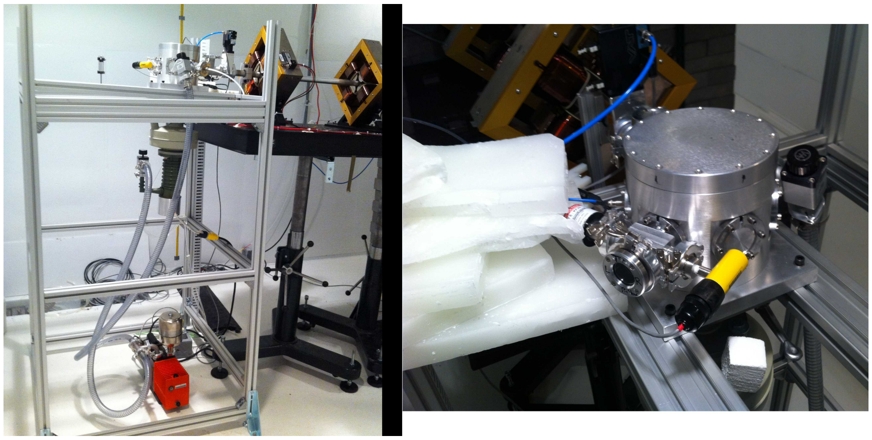

Figure 4.4 Left: An image of the assembled experimental chamber, vacuum system and diagnostics. Right: An image of the experimental chamber.

The experimental chamber (see Figure 4.5) was machined out of aluminum 6061. It has 6 KF 40 bulkhead mounts arrayed 60 degrees about the side of the chamber. A 1/4-20 breadboard was machined on the internal face of the chamber lid.

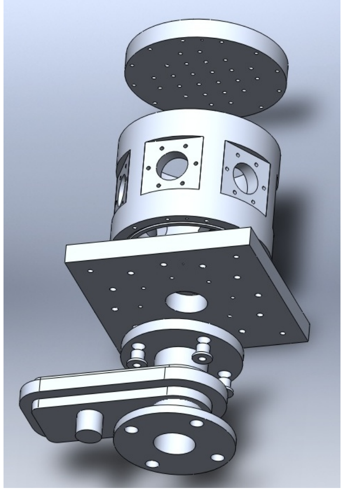

Figure 4.5 3D exploded view of the experimental chamber with the isolation valve.

The experimental chamber is pumped down to a high vacuum with a Varian M2 oil diffusion pump backed with an Alcatel 2021A mechanical pump. An aluminum gate valve and liquid nitrogen baffle isolate the experimental chamber from the vacuum system. Two Varian gate valves enable the chamber to be roughed, bypassing the oil diffusion pump. The oil diffusion pump is cooled with the Neslab RTE-9DD chiller shown below in Figure 4.6.

Figure 4.6 The Neslab chiller used to cool the M2 oil diffusion pump.

The Terra Nova 960 CCG/CVT (pirani gauge, cold cathode gauge) pressure controller monitors the experimental chamber pressure.

A KF 40 BNC feedthough monitors the beam current on target. A Ceramic target holder electrically isolates the sample from the chamber. A KF 40 glass view enables visual inspection inside the experimental chamber during experiments. A KF 40 gas feedthough purges the chamber with nitrogen; it has a 1/4" compression fitting. A needle valve bleeds nitrogen into the chamber.

4.1.4 Beam Imaging System

An image of the beam imaging setup is shown in Figure 2.

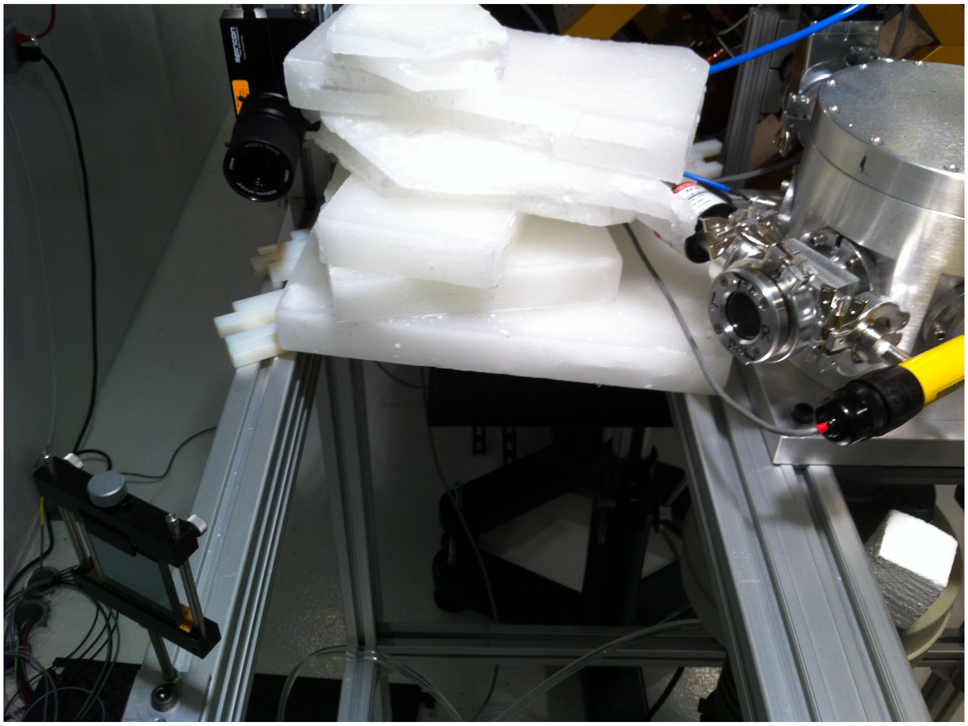

Figure 4.7 Image of the beam imaging setup.

The inside of the vacuum chamber is shown in Figure 4.8. An aluminum mask and YAG crystal are positioned at the front of the chamber; an enlarged view is shown in Figure 4.9. The YAG crystal scintillates (creates visible light) when struck with a charged particle beam. The crystal is angled about 15 degrees from parallel to the beam to make it easier to view with a camera. A viewport and mirror direct the scintillated light to a high pixel density camera. The intensity of light is directly proportional to the proton beam flux. The small ticks and large ticks in the mask are 1mm and 2mm long respectively. A CAD drawing of the mask is shown in Figure 6.1.

An image plane is generated in real-time using a scintillator composed of a Ce:YAG crystal (1.5 in diameter, 100 um thick) and an aluminum mask (1.5 in diameter, 50 um thick). A Spiricon SP620U USB camera with a Techspec 75 mm focusable double gauss macro captures the image plane of the aluminum mask; the image is processed with BeamGage standard version 5.5.

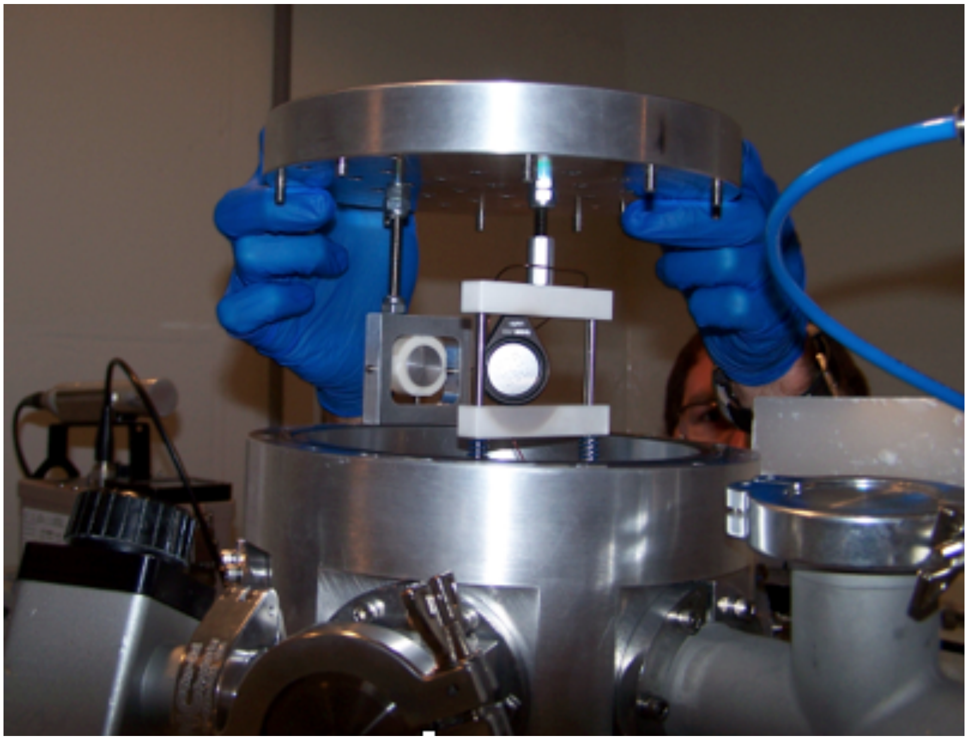

Figure 4.8 Image of the vacuum chamber housing the YAG crystal and faraday cup.

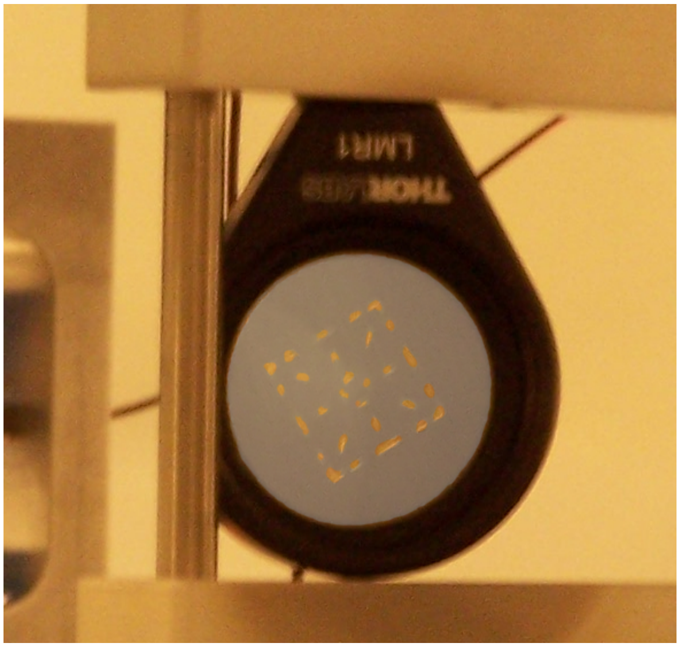

Figure 4.9 Image of the mask and YAG crystal.

4.1.5 Beamline Control and Data Acquisition

The electronics control tower for the beamline is shown below in Figure 4.10. Instrument #1 is a TerraNova pressure controller; it monitors the experimental chamber pressure. Instrument #2 is a Keithley picoampemeter and it monitors the beam current. Instrument #3, #4, and #5 are Kepco ATE 25-20 DC power supplies and they drive the current through each quadrupole. Instrument #6 is a switch panel. A wiring diagram for the electronics tower is given in appendix C.

Figure 4.10 Electronics tower for the beamline

A LabVIEW program (see Figure 4.11) controls the magnets and collects the experimental data during irradiations. Three control panels in the top left corner of the virtual instrument (VI) supply a 0-1V signal to the power supplies. The signal linearly drives the power supplies from 0-20A. However, a 500 ohm resister was installed in each power supply to limit the total current to approximately 12A. The output current of each power supply is monitored by the voltage across a reference resister inside the power supplies. The voltage drop across the resisters is imported into LabVIEW and recorded as a function of time. The current driven through each magnet is displayed in real-time in the top left of the VI, it is also charted in the bottom left, and is written to a file when the WRITE button is clicked.

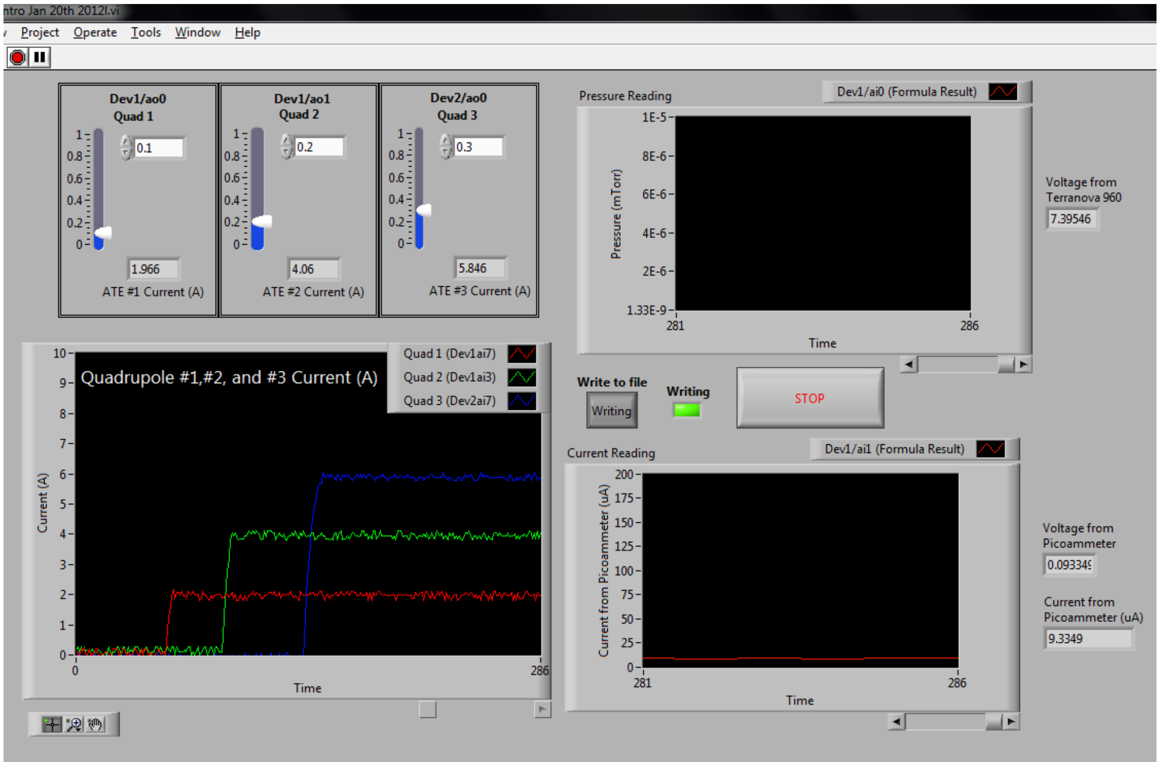

Dev1/ao0 Quad 1: 0.1
ATE #1 Current (A): 1.966

Dev1/ao1 Quad 2: 0.2
ATE #2 Current (A): 4.06

Dev2/ao0 Quad 3: 0.3
ATE #3 Current (A): 5.846

Voltage from Terranova 960: 7.39546

Voltage from Picoammeter: 0.09334(

Current from Picoammeter (uA): 9.3349

Figure 4.11 The LabVIEW virtual instrument program used to control the quadrupoles and acquire data.

A signal from the TerraNova pressure controller is charted in the top right of the VI and can be written to a file. A signal from the Keithley picoampemeter is charted in the bottom left of the VI and can be written to a file. LabVIEW writes the data to a file every 0.5 seconds when the WRITE button is green. A standard operating procedure to operate to beamline using LabVIEW and the power tower is given in appendix C.

Chapter 5

Beamline Alignment and Characterization

5.1 Beamline Alignment

5.1.1 Introduction

This section covers the work to center the cyclotron beam down the beamline. The beam needs to be centered down the entire beamline to limit the amount of beam current lost due to collision with the beamline sidewalls. Also the quadrupoles will steer the beam if it is not centered down the beamline, and this steering will further reduce the total current on target. The approach taken was similar to sighting in a rifle: aim, fire, look at target, adjust sights, and repeat.

Over the course of six months the beamline was aligned. A list of the alignment experiments is shown below in Table 5.1. The tables and figures for the experiments are very large and where put in appendix D. We had trouble aligning the beam by this method, and hypothesized that the beam characteristics were changing over the course of six months. Therefore, while we were trying to center the beamline we also collected data on the stability and the control of the beam; this was accomplished by changing the stripping foil position and observing the effects it had on the beam down the beamline.

Table 5.1 List of experiment conducted to align the beamline.

Alignment Experiment	Date	Goal	Table	Figure
Trial #1	June 23rd, 2011	**1**	--	Figure 6.4
Trial #2	August 15th, 2011	**1**	Table 6.1	Figure 6.5
Trial #3	August 31st, 2011	**1,2**	Table 6.2	Figure 6.6
Trial #4	September 19th, 2011	**1**	Table 6.3	Figure 6.7
Trial #5	September 27th, 2011	**1**	Table 6.4	Figure 6.8
Trial #6	September 28th, 2011	**1**	Table 6.5	Figure 6.9
Trial #7	September 29th, 2011	**3**	Table 6.6	Figure 6.10
Trial #8	October 7th, 2011	**1**	Table 6.7	Figure 6.11
Trial #9	November 16th, 2011	**3**	Table 6.8	Figure 6.12
Trial #10	November 17th, 2011	**3**	Table 6.9	Figure 6.13
Trial #11	December 14th, 2011	**1,4**	Table 6.10 Table 6.12 Table 6.12	Figure 6.14 Figure 6.15

Goal: **1**-Center the cyclotron beam down the beamline
2-Compare paper burns to radiochromic film burns
3-Determine the stripping foil effect on the beam trajectory
4-Demonstrate the focusing ability of the quadrupole triplet

5.1.2 Experimental

The cyclotron beam was extracted out of the second target port; the beam has a 2° incline from the horizontal exiting this port. To roughly align the beamline a laser level, adjusted to have a 2° decline, was positioned at the end of the vault. The height of the laser level was adjusted until the laser was centered on the 2nd target port. The long drift tube was run though the quadrupole triplet and the short drift tube was added to the beamline. The drift tube must be 10 inches from the bottom of the table to be centered in the quadrupoles. The long drift tube height was set to 10 inches above the table surface, and the table legs were adjusted to reposition the long drift tube portion of the beamline. A support structure that runs from the cyclotron to the concrete wall holds the short drift tube in place. The short drift tube position was adjusted on this support structure.

The short drift tube position was adjusted until the laser beam was centered at both ends of the tube. With the short drift tube secured to the support structure the long drift tube position was adjusted until the laser beam was center on both ends of the tube. The table height was tricky to adjust due to the need for the beamline to be at a 2° incline. The long drift tube and short drift tube were connected and then evacuated by the cyclotron. Finally, with the beamline roughly aligned the laser level was removed and the cyclotron beam was "sighted in".

"Sighting in" was a multiple stage process. The points in the beamline that were used to measure the cyclotron beam are shown below in Figure 5.1.

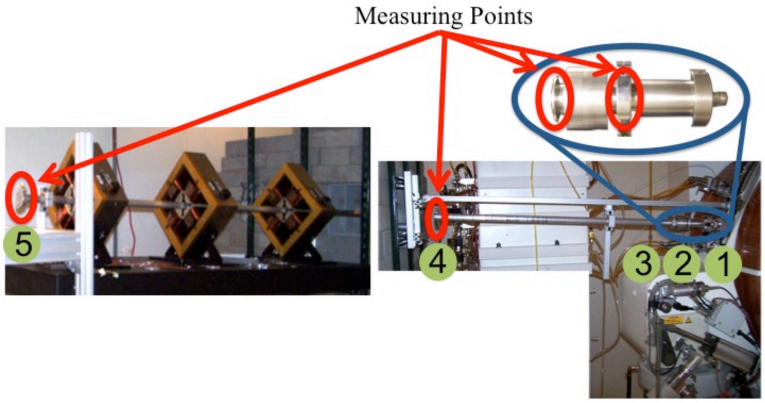

Figure 5.1 A schematic of the points used to measure the beam profile during beamline alignment.

Table 5.2 A description for the locations depicted in Figure 5.1

Location	Description	Length from cyclotron (in)
1	cyclotron 2nd target port exit	0
2	after KF40 cyclotron adapter	4
3	after collimator	7.25
4	after short drift tube	49.25
5	after long drift tube	139.25

The origin of the beamline coordinates was set to the 2nd target port of the cyclotron (Location 1). Initially, measurements of the beam were taken, without the collimator in the beamline; these measurements were taken after the KF40 cyclotron adapter (Location 2), and after the short drift tube (Location 4). The collimator was added to the beamline once the beam was centered at the end of the short drift tube (Location 4). The collimator was used to reduce the beam diameter so that it would be easier to center. The collimator, shown below in Figure 5.2, has three orifice diameters: 0.5 mm, 1 mm, and 3 mm. It can also be used without an orifice.

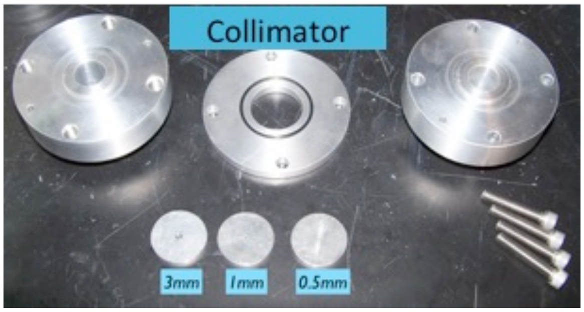

Figure 5.2 The collimator used to reduce the beam spot size during beamline alignment.

With the collimator installed, the reduced cyclotron beam was centered after the short drift tube (Location 4). Then the long drift tube was added and the beam was centered at the end of the long drift tube (Location 5).

The aluminum KF40 blank flange, shown in Figure 5.3, was machined to 0.5 mm thick and modified to make the beam measurements more repeatable and easier for operators to use; this modified blank flange was added to the beamline measurement on September 27th, 2011. All beam alignments done before September 27th used a KF40 blank flange that was 1.5 mm thick.

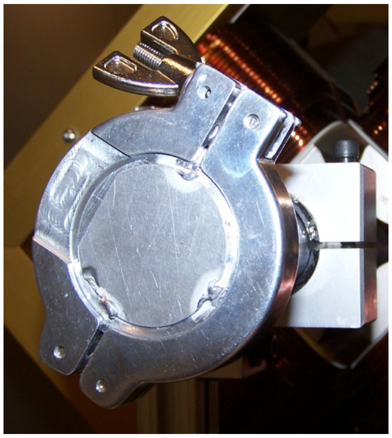

Figure 5.3 The modified KF40 blank flange.

Therefore images of the cyclotron beam were taken by varying the stripping foil position. During these experiments the position of the beamline was fixed so that any change in the beam profile would be due to the change in the stripping foil position.

Almost all the beam profiles images were measured by placing radiochromic film directly in the proton beamline. The beam intensity cannot be quantified spatially by this method due to the film being over developed. However, it is a great tool for quickly identifying the beam position due to it being much easier to see than paper burns.

Once the beam was centered down the entire beamline, the quadrupole magnets were turned on and the current of the magnets were adjusted. The goal of this experiment was merely to see if the magnets would focus the proton beam.

5.1.3 Results and Discussion

5.1.3.1 Trial #3

The beam profiles B1 to R1.4 were acquired with the stripping foil position at 52% (Figure 6.6). The paper beam profiles B1, B1-2, and B1-3 appear to be in the same position but B1-2 and B1-2 are darker in color. The darker color is due to the extended irradiation times. The film beam profiles R1.1 through R1.4 appear to have similar shape and intensity. The darker halo in R1.4 is due to the increased irradiation time. The paper beam profiles show the beam striking the center of the KF40 blank flange but the film beam profiles show the beam striking the lower half of the KF40 blank flange. It is unclear why paper and film give different beam positions.

The beam profiles B3 to R3.3 were acquired with the stripping foil position at 54%, (Figure 6.6). The paper beam profiles B3, B3-2, and B3-3 appear to be in the same position but vary in color, which is due to over exposure of the film. The film beam profiles R3.1, R3.2, and R3.3 have the same shape and intensity. They each have a dark halo above the very dark beam image. The paper beam profiles show the beam striking the top of the KF40 blank flange but the film beam profiles show the beam striking the entire target area. The proton beam is high which is causing the dark halo in the film beam profiles. The large beam profiles in the film images are due to the proton beam scattering off the top of the KF40 adapter.

At a stripping foil position of 52% the beam appears low from center, as the stripping foil position increases to 54% the beam position becomes high from center. The beam position was difficult to determine because the entire detection area of the film was changing color. To solve this problem the collimator in Figure 5.2 was machined to reduce the beam size, and make it easier to align the beamline.

5.1.3.2 Trial #4

The experimental array and film beam profiles are shown in Table 6.3 and Figure 6.7, respectively. Initially the beam was low from center, but by adjusting the stripping foil position and drift tube position the beam was roughly centered, see images R10 and R11. It was difficult to determine the collimated beam location relative to the center of the drift tube. A new target holder was made to hold the film in the same orientation and position, see Figure 5.3.

5.1.3.3 Trial #5

The experimental array and film beam profiles are shown in Table 6.4 and Figure 6.8, respectively. The beam was centered down the short drift tube. The halo above the small beam ellipse in each film beam profile was due to the beam scattering off the bottom of the collimator. The beam profile in B1 through B10 is the same size and shape. The beam divergence is seen with the addition of the long drift tube. The beam profile in F1 and F2 has the same shape as B1 through B10 but is larger because due to the beam divergence. Image F1 shows the beam nearly center down the entire beamline.

5.1.3.4 Trial #6

The experimental array and film beam profiles are shown in Table 6.5 and Figure 6.9, respectively. The experimental setup for F1 (Table 6.4) and A1 (Table 6.5) are exactly the same. However, the beam images (Figure 6.8 and Figure 6.9) are very different. The beam in F1 appears much weaker than A1, and A1 was activated. The sudden change in the beam intensity is believed to be caused by the stripping foil or ion source of the cyclotron.

The beam profile in A1 through A4 is elongated in the bending plane of the cyclotron. The beam travels through a 0.5 mm diameter but the beam profiles are very elliptical. The elongation in the beam profile is due to the beamline not being parallel to the beam. The top of the beam scatters of the top wall of the collimator which reflects the beam down; this causes the extreme elongation. Scattering off the collimator wall is seen easily in beam profile A9. The dark circular object is the beam and the blurry spot below it is scattering from the top wall of the collimator.

5.1.3.5 Trial #7

The experimental array and film beam profiles are shown in Table 6.6 and Figure 6.10, respectively. The beam profile measurements on August 31, 2011 showed that the proton beam moves up as the stripping foil increases from 52-54%, however, there was no way to determine if the angle of the beam exiting the cyclotron changed too. The addition of the drift tubes and the collimator made it possible to determine if the beam angle changed as the stripping foil position changed, and is described shortly. Beam profiles C1 through

C9 were taken at the end of the long drift tube after the beam traveled through a 0.5 mm diameter collimator.

C7 was taken with the stripping foil position at 50%, the beam strikes the very top of the film. When stripping foil position was set to 52%, the beam profiles, shown in C1 and C2, increase in intensity and size; the beam has also moved down on the film. Slightly above a stripping foil position above 52%, the beam profiles, shown in C4, C6, and C9, have less intensity and have multiple locations where the film changed color. Finally, increasing the stripping foil position to 53% created a beam profile, shown in C3, that has a reduced intensity and a lower position on the film.

The cyclotron beam angle increases as the stripping foil position increases from 50% to 53%. The top of the beam travels through the collimator when the stripping foil position is low and the beam is scattered off the bottom of the collimator. The beam intensity is greatest when the center of the beam travels through the collimator. The beam is scattered of the top of the collimator when the stripping foil is high and scattered to the bottom of the film. The beam angle increases slightly as the stripping foil position increases.

5.1.3.6 Trial #8

The experimental array and film beam profiles are shown in Table 6.7 and Figure 6.11, respectively. Beam profile X4 shows the beam centered down the short drift tube. Beam profile X8 shows the beam centered down the long drift tube.

5.1.3.7 Trial #9 & Trial #10

The current on collimator 1/2 (lower collimator) decreased from 50% to 0% of the foil current as the stripping foil position changed from 50.5% to 53%. While the current on collimator 2/3 (upper collimator) increased from 0% to 25% of the foil current as the stripping foil position changed from 50.5% to 53%. The diagram in Figure 5.4 shows the position of the collimator 1/2 and collimator 2/3 relative to the beam.

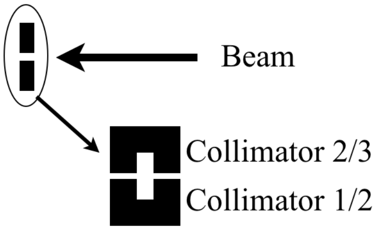

Figure 5.4 A diagram of the position of the cyclotron's collimators

At the collimators the beam moves up as the stripping foil position increases. The collimated beam travels through a 0.5 mm orifice and then drifts to the film at the end of the long drift tube. Visual inspection of the beam images in Figure 6.12 and Figure 6.13 shows the beam striking relatively the same position regardless of the stripping foil position. Therefore the angle of the beam remains constant. Visual inspection of Figure 6.12 and Figure 6.13 show the maximum intensity of the beam around 51.5% and 52%.

5.1.3.8 Trial #11

Image Short 2 shows the beam centered down the short drift tube image Long 3 shows the beam centered down the long drift tube, see Figure 6.14. The shape of the beam in image Long 2 is due to the beamline not being strait and the beam striking the drift tube sidewall. The shape of the beam in image Long 3 is due to the shape of the Cyclotron collimators. It is interesting that this image is produced after it travels through a 0.5 mm orifice.

The quadrupole current experimental array and beam images are shown in Table 11 and Figure 18, respectively. The beam in Long Mag 1 is elliptical with the major radius vertical and the beam is focused to a point by increasing the current of the quadrupoles, see Long Mag 2 through Long Mag 7.

Long Mag 2 to Long Mag 6 shows the beam is steered down and slightly left. The left-right position of each quadrupole was adjusted to correct the horizontal displacement of the beam. The quadrupole support table was raised to correct the vertical steering of the beam. Image Long Mag 7 showed the beam closer to center after repositioning of the quadrupoles and their support table.

The 0.5 mm orifice was removed for Long Mag 8 through Long Mag 11. The films are much darker due to the increase in current and increased beam size. Image Long Mag 8 showed that the beam is no longer a point but rectangular. Increasing the current from Long Mag 8 to Long Mag 10 yielded a larger beam. The beam is expanding because the focal point is in front of the film. Image Long Mag 11 showed a tight elliptical beam with the major radius in the vertical plane.

5.2 Beam Characterization

5.2.1 Experimental

On Jan 24th 2012 the cyclotron beam profile was captured in real-time using the YAG beam diagnostic and LabVIEW recorded the current driven through each quadrupole. On Jan 31st, 2012 two HAVAR foils (each foil is roughly 20 um thick) were added to the beamline, and the beamline length increased slightly due to the addition of the HAVAR foil holder. To cool the foils helium gas flows (roughly 5 liters/sec, 50 psi) between them. The helium window is 1.25 in thick. Both days, the chamber pressure was maintained below $5x10^{-5}$ torr.

5.2.2 Results and Discussion

Figure 5.5 shows the beam profile as the stripping foil was swept from 50.8% to 53%, by 0.1% increments. The beam had the best intensity between 51.9% and 52.6%, and was centered between 52.2% and 52.4%. The stripping foil position was set to 52.3% for the remaining experiments.

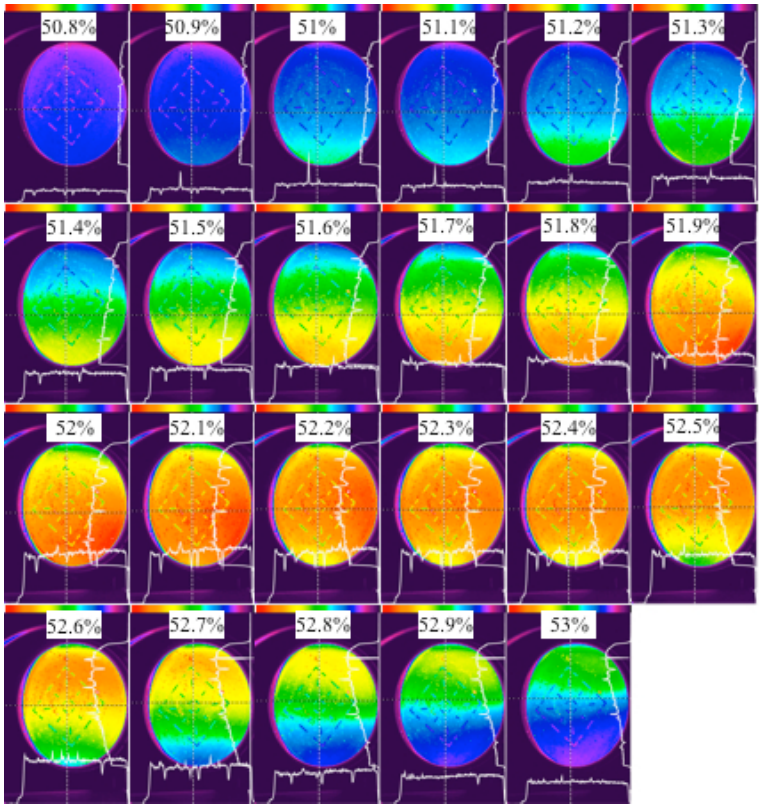

Figure 5.5 Realtime images of the cyclotron beam as the stripping foil is adjusted captured with the YAG crystal diagnostic. Images were taken on January 24th, 2012.

Beam profiles were taken as the current driven through each quadrupole was changed and are shown in Figure 5.6 and Figure 5.8. The spot size and intensity of the beam was strongly dependent on the current driven in each quadrupole, see Figure 5.7 and Figure 5.9. A spot size of about 2 mm in diameter (Figure 5.6 image #12) was achieved on Jan 24th 2012 when the current settings were 6.8, 7.2, and 11.4 amperes for quadrupole #1, quadrupole #2, and quadrupole #3, respectively.

For the images taken on Jan 31st 2012, the beam was found to compress vertically when the current driven through each quadrupole was about 4 amperes. The best focus (Figure 5.8 image #14) achieved a 6 mm diameter spot when the current driven through the first, second, and third quadrupole was 3.2, 6.2, and 8.3 amperes, respectively. These currents correspond to a magnetic field gradient of 4.2, 9.5, and 12 tesla per meter. Presently, the first and second quadrupole appear to only focus while the third also steers the beam. Beam steering is due to a slight misalignment of the third quadrupole.

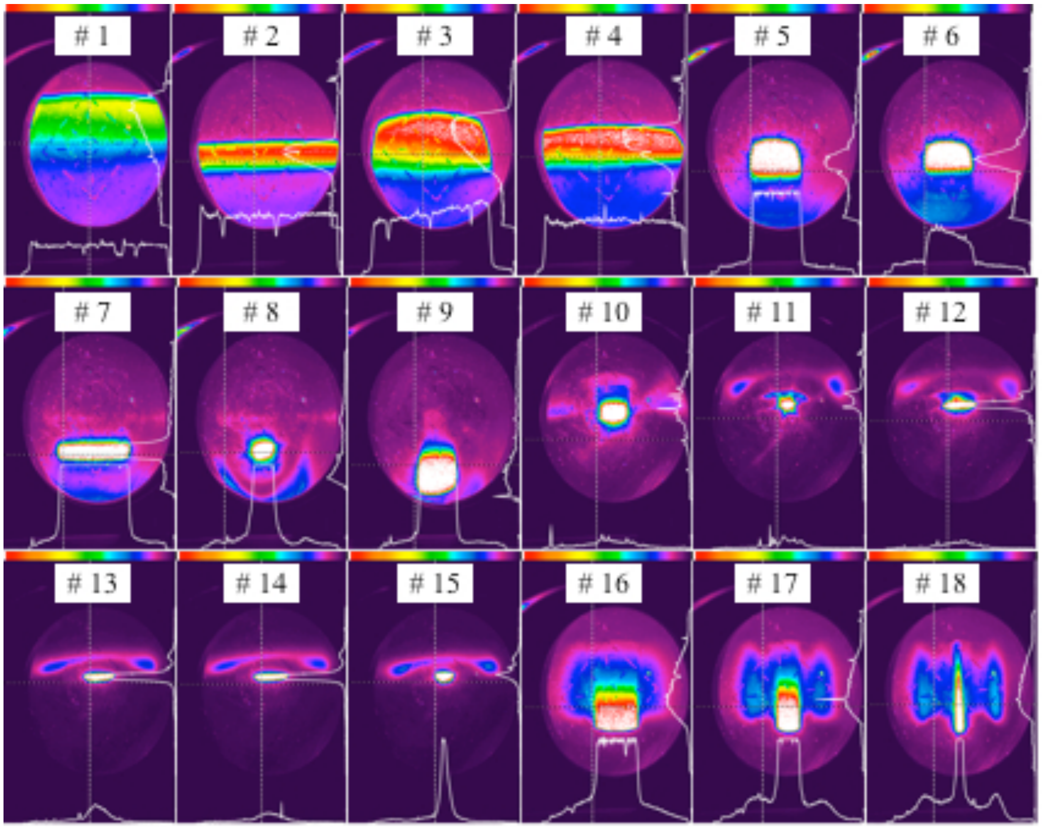

Figure 5.6 Realtime images of the focused cyclotron beam captured with the YAG crystal diagnostic. Images taken on January 24th, 2012.

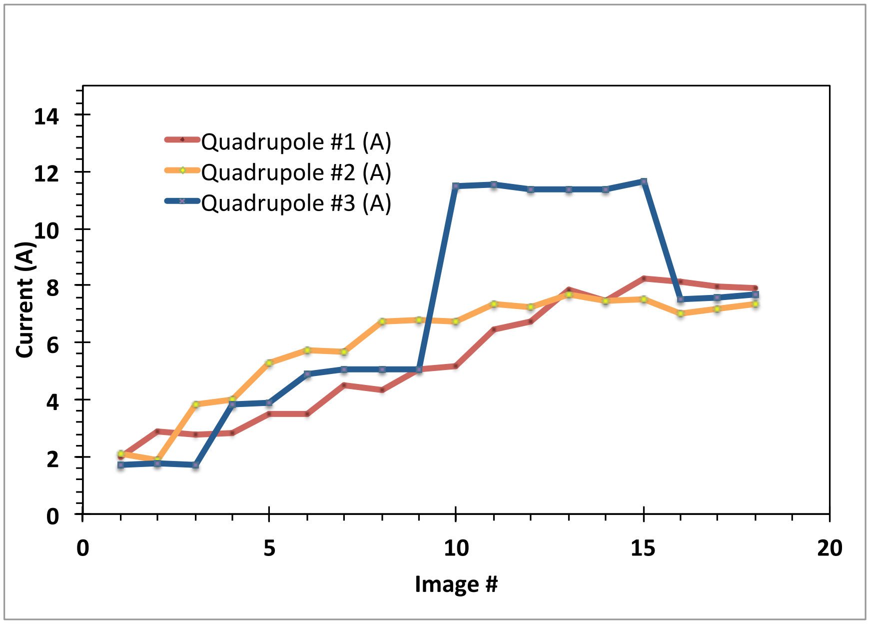

Figure 5.7 ***Quadrupole current of images slices taken on January 24th, 2012.***

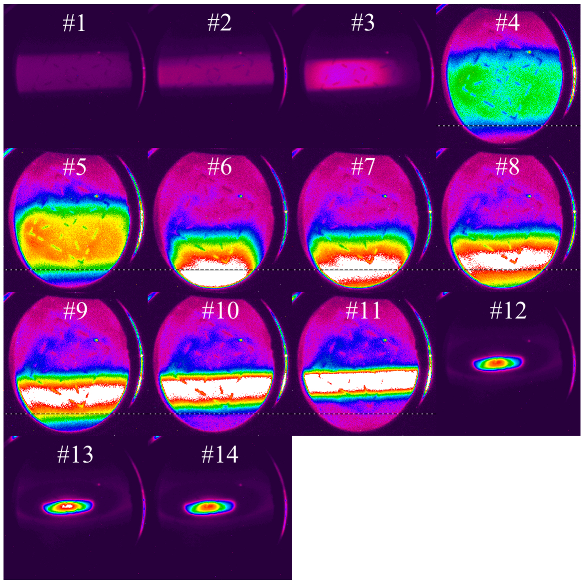

Figure 5.8 ***Realtime images of the focused cyclotron beam captured with the YAG crystal diagnostic. Images taken on January 31st, 2012.***

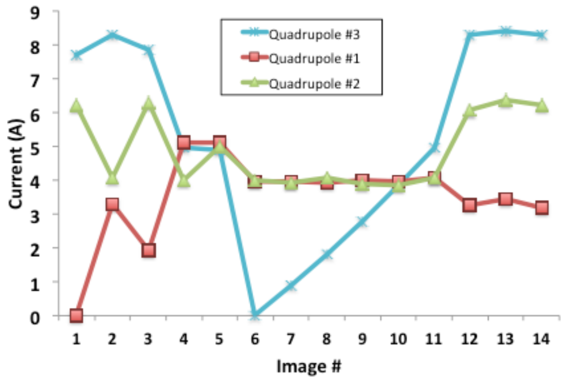

Figure 5.9 Quadrupole current of image slices taken on January 31st, 2012.

The beam was found to compress vertically when the current through each quadrupole was about four amperes. The best focus was achieved with a current of 3.2, 6.2, and 8.3 amperes through the first, second, and third quadrupole, respectively. These currents correspond to a magnetic field gradient of 4.2, 9.5, and 12 tesla per meter. The red portion of the beam in image #14 is about 1mm in diameter.

The stability of the beam was a concern; we thought the beam might drift over time due to the ion source and the magnetics changing during operation. Below in Figure 5.10 is the focus beam profile before and after forty-five minutes of operation. The beam demonstrated great stability and did not appear to drift after forty-five minutes. The target current slowly increased with time. Adjustments were made to the ion source of the cyclotron to compensate for drift in the current.

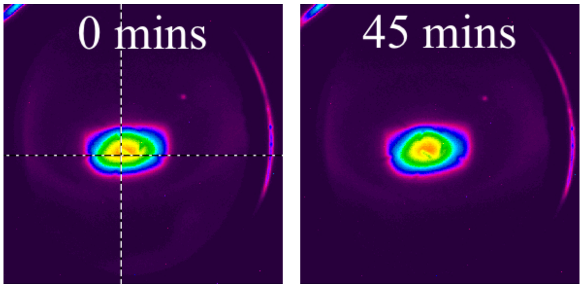

Figure 5.10 Comparison of the focused beam after forty-five minutes of operation.

A comparison of the beam profile as the stripping foil current increases from 1.6 uA to 7.1 uA is shown in Figure 5.11. The beam size, location, and distribution remained constant as the current increased.

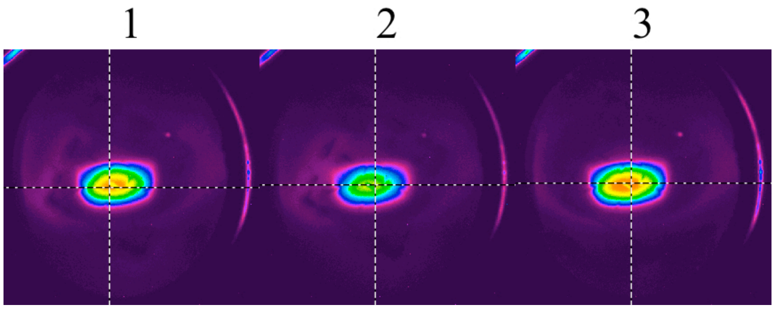

Figure 5.11 Comparison of the beam profile as the stripping foil current increases. Images taken on January 31st, 2012.

A comparison of the focused beam profile with and without HAVAR foil in the beamline are shown in Figure 5.12. In both images the majority of the beam intensity is in a 2 mm diameter. However, the beam profile with HAVAR foils much more dispersed. The beam dispersion is due to attenuation of the beam as it travels through the HAVAR and helium gas.

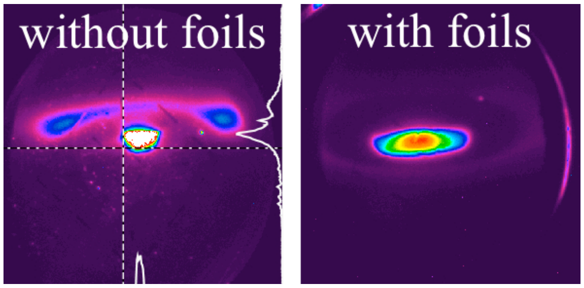

Figure 5.12 Comparison of the focused beam profile with HAVAR foil windows and without HAVAR foil windows. Left: Image taken on Jan 24th 2012. Right: Image taken on January 31st, 2012.

5.2.3 Conclusion

The current needed to focus the beam is strongly dependent on the location of each magnet. Currently, the first and second quadrupole appear to only focus while the third also steers the beam. Steering of the cyclotron beam is due to misalignment of the third quadrupole. The data demonstrates that the beamline is capable of focusing the proton beam to a 4 mm spot with most of the beam intensity residing in a 1mm diameter spot. The focused beam showed stability during forty-five minutes of operation. The target current drifted during operation but could be fixed by adjusting the ion source of the cyclotron.

Chapter 6

Recommendations

6.1 Ion Optics Upgrade

A bending magnet would be a great addition to the beamline. It would allow the beamline to be horizontal, and correct change in the beam trajectory due to variation in the ion source or stripping foil. This magnet would also reduce the amount of dose workers receive. A larger bore beamline would reduce the amount of beam loss due to the beam striking the sidewalls of the drift tubes; this would increase the total flux on target.

6.2 Beam Diagnostics & Sample Mount

Modify the YAG imaging system so that it can actuate in and out of the beamline. In the current configuration the YAG is exposed to high beam currents during experiments; this is unnecessary and damages the YAG crystal.

Design and install a rotary carousel that houses the samples and diagnostics. Ideally, a graphite beam dump would be located in the center and samples could be positioned radially. The YAG crystal could also be in one of the positions. The YAG could be used initially to see the beam during startup and focusing. Then the samples could be moved in and out of the beam. All the while the beam dump is recording the total current.

Add graphite beam slits to the beamline. The slits will help during alignment operation, and also reduce the amount of equipment activation due to beam spill.

6.3 Automation

Write an automated degaussing program to degauss the magnets. This would eliminate any human error and make it simple for operators to use. Currently, this is done manually and the effectiveness is unknown. Also, write an automated focusing program that would automatically find the optimum current to drive through each magnet. This would reduce the cost of an experiment because it would eliminate the time spent tweaking the beam.

6.4 General

Run the VAT valve position indicator wire and hook up a LED light to it so the valve position is known at all times.

In the current setup, the quadrupole triplet is still able to focus the proton beam, but the 3rd quadrupole triplet is slightly misaligned. Aligning the 3rd quadrupole would increase the beam current on target, and also eliminate beam steering.

References

1. Avila-Rodriguez, M. A.; Wilson, J. S.; McQuarrie, S. A., The use of radiochromic films to measure and analyze the beam profile of charged particle accelerators. *Appl. Radiat. Isot.* **2009,** *67* (11), 2025-2028.

2. (a) Dahl, D. A. *SIMION 3D VERSION 7.0 USER'S MANUAL*; 2000; (b) Dahl, D. A., SIMION PC/PS2 electrostatic lens design program. *Rev. Sci. Instrum.* **1990,** *61* (1), 607-609.

3. Legge, G. J. F., A history of ion microbeams. *Nuclear Instruments & Methods in Physics Research, Section B: Beam Interactions with Materials and Atoms* **1997,** *130* (1-4), 9-19.

4. Humphries, S., *Principles of Charged Particle Acceleration*. John Wiley and Sons: 1999.

5. GE_Healthcare *PETtrace 800 series SERVICE MANUAL – ACCELERATOR*; GE Healthcare: 2011.

6. (a) Dehnel, M. P.; Trudel, A.; Duh, T. S.; Stewart, T., Beamline developments in commercial cyclotron facilities. *Nuclear Instruments & Methods in Physics Research, Section B Beam Interactions with Materials and Atoms* **2005,** *241* (1-4), 655-659; (b) Dehnel, M. P.; Jackle, P.; Roeder, M.; Stewart, T.; Theroux, J.; Brasile, J. P.; Sirot, P.; Buckley, K. R.; Bedue, M., A compact cost-effective beamline for a PET Cyclotron. *Nuclear Instruments & Methods in Physics Research, Section B Beam Interactions with Materials and Atoms* **2007,** *261* (1-2), 809-812; (c) Dehnel, M. P.; Dawson, R. J.; Pattyn, E.; Stinson, G. M.; Helmer, R.; Keitel, R.; Dale, D.; Wilson, A. In *The design and operation of an industrial beam transport system for 15-30 MeV protons*, Industry

Applications Society Annual Meeting, 1991., Conference Record of the 1991 IEEE, 28 Sep-4 Oct 1991; 1991; pp 1374-1380 vol.2; (d) Stokely, M.; Wieland, B.; Hill, C.; Dehnel, M. P.; Stewart, T. M., A High Current PET Target and Compact Beamline. In *PAC09*, Vancouver, British Columbia, Canada, 2009; p 2808; (e) M. P. Dehnel; T. Stewart; T. S. Duh, Industrial Beamline Design for Radioisotope Production. In *CYC2004*, Tokyo, Japan, 2004; p 486; (f) Dehnel, M. P., Industrial Beamline Technologies And Approaches. *AIP Conf. Proc.* **2011,** *1336* (1), 21-25; (g) M. P. Dehnel; J. E. Theroux; T. Christensen; T. M. Stewart, Measurements from a Compact Cost-Effective Beamline for the THC14 PET Cyclotron. *AIP Conf. Proc.* **2009,** *1099* (Application of Accelerators in Research and Industry), 504-507; (h) J. E. Theroux; M. P. Dehnel; P. T. Jackle; M. Roeder, A 'Short Port' Beamline for Mounting Custom Targets to a GE PETtrace^{TM} Cyclotron. In *CYC2007*, Giardini Naxos, Italy, 2007; p 361.

7. B.F. Milton; *et al.* In *Commissioning and First Operation of a 500 uA, 30 MeV H Cyclotron: The TR30*, IEEE Particle Accelerator Conference, San Francisco, California, San Francisco, California, 1991; p 65.

8. Products, I. S. GAFCHROMIC® EBT2 Dosimetry Film. http://online1.ispcorp.com/%5Flayouts/Gafchromic/content/products/ebt2/pdfs/EBT2productSpec.pdf (accessed March 3rd).

9. Arjomandy, B.; Tailor, R.; Anand, A.; Sahoo, N.; Gillin, M.; Prado, K.; Vicic, M., Energy dependence and dose response of Gafchromic EBT2 film over a wide range of photon, electron, and proton beam energies. *Med Phys* **2010,** *37* (5), 1942-1947.

10. Cheung, T.; Butson, M. J.; Yu, P. K. N., Post-irradiation colouration of Gafchromic EBT radiochromic film. *Phys Med Biol* **2005,** *50* (20), N281.

11. Richley, L.; John, A. C.; Coomber, H.; Fletcher, S., Evaluation and optimization of the new EBT2 radiochromic film dosimetry system for patient dose verification in radiotherapy. *Phys Med Biol* **2010,** *55* (9), 2601.

Appendix A

6.5 SIMION Fly Program

```
;------------------------------------------------------------------

; this user program randomly changes the initial ke and direction of ions

; energy is randomly changed +- Percent_Energy_Variation * ke

; ions are emitted randomly within a cone of revolution around the

; ion's defined velocity direction axis

; the full angle of the cone is +- Cone_Angle_Off_Vel_Axis

; (e.g. 90.0 is full hemisphere, 180 is a full sphere)

;------------------------------------------------------------------

 ;--------- you can use it with your own lenses without modification ----------

;           (just rename user program file using your pa's name)

;------ Note: you can also modify the emission distributions as desired ------

defa Percent_Energy_Variation     2    ; (+- 2%) random energy variation

defa Beam_divergence_mrad         3.5

seg initialize                         ; initialize ion's velocity and direction

      ;------------------ get ion's initial velocity components ------------
```

```
rcl ion_vz_mm                 ; get ion's specified velocity components

rcl ion_vy_mm

rcl ion_vx_mm

 ;------------------ convert to 3d polar coords ------------

>p3d                          ; convert to polar 3d

 ;------------------ save polar coord values ---------------

sto speed rlup                 ; store ion's speed

sto az_angle rlup              ; store ion's az angle

sto el_angle                   ; store ion's el angle

 ;------------------ make sure Percent_Energy_Variation is legal -------------

                       ; force 0 <= Percent_Energy_Variation <= 100

  rcl Percent_Energy_Variation abs

100 x>y rlup sto Percent_Energy_Variation

 ;------------------ make sure Cone_Angle_Off_Vel_Axis is legal -------------

                       ; force 0 <= Cone_Angle_Off_Vel_Axis <= 180

rcl Beam_divergence_mrad 1000 / 360 * 2 / 3.14159265358979 /

sto Cone_Angle_Off_Vel_Axis
```

```
rcl Cone_Angle_Off_Vel_Axis abs
180 x>y rlup sto Cone_Angle_Off_Vel_Axis
 ; --------------------- calculate ion's defined ke -------------
rcl ion_mass                  ; get ion's mass
rcl speed                     ; recall its total speed
>ke                           ; convert speed to kinetic energy
sto kinetic_energy            ; save ion's defined kinetic energy
 ; --------------------- compute new randomized ke -------------
                              ; convert from percent to fraction
rcl Percent_Energy_Variation 100 /
sto del_energy 2 * rand *     ; fac = 2 * del_energy * rand
rcl del_energy - 1 +          ; fac += 1 - del_energy
rcl kinetic_energy *          ; new ke = fac * ke
 ; --------------------- convert new ke to new speed -----------
rcl ion_mass                  ; recall ion mass
x><y                          ; swap x any y
>spd                          ; convert to speed
```

```
sto speed                ; save new speed



;-- compute randomized el angle change 90 +- Cone_Angle_Off_Vel_Axis -------

;-------- we assume elevation of 90 degrees for mean ---------

;-------- so cone can be generated via rotating az +- 90 -------

                     ; (2 * Cone_Angle_Off_Vel_Axis * rand)

2 rcl Cone_Angle_Off_Vel_Axis * rand *

                     ;  - Cone_Angle_Off_Vel_Axis + 90

rcl Cone_Angle_Off_Vel_Axis - 90 +

 ;------------- compute randomized az angle change ------------

;--------- this gives 360 effective because of +- elevation angels ---

180 rand * 90 -            ;        +- 90 randomized az

 ;--------------------- recall new ion speed ------------------

rcl speed                ; recall new speed

 ;--------- at this point x = speed, y = az, z = el --------------

;------------ convert to rectangular velocity components ---------

>r3d                     ; convert polar 3d to rect 3d
```

```
 ;------------ el rotate back to from 90 vertical -------------
-90 >elr
 ;------------ el rotate back to starting elevation -------------
rcl el_angle >elr


;------------ az rotate back to starting azimuth -------------
rcl az_angle >azr
 ;------------ update ion's velocity components with new values --------
sto ion_vx_mm              ; return vx
rlup
sto ion_vy_mm              ; return vy
rlup
sto ion_vz_mm              ; return vz
 ;--------------------- done --------------------------------------
```

6.6 Quadrupole Scaling Program File

```
;----------------------------------------------------------------
; this program file changes the magnetic field though a 300 mm quadrupole to have a
gaussian distribution------------------------------------------
Defa a 1.01875447275549
Defa b 1087.45880138474
Defa c 479.163407263729
Seg Mfield_Adjust
RCL Ion_Pz_gu ABS STO location
1190 RCL location
X<Y EXIT GSB Bcalc


LBL Bcalc
RCL c ENTER * 2 *                                   ;      2c^2
1/X STO temp1                             ;      1/(2c^2)
RCL location RCL b - ENTER * STO temp2    ;      (x-b)^2
RCL temp1 RCL temp2 * -1 *                          ;      -(x-b)^2/(2cc)
```

```
E^X                                                     ;       exp(value above)

RCL a *                                                 ;        a*(value above)

STO probfunct                                           ;       probability function

RCL Ion_BfieldX_gu RCL probfunct * STO Ion_BfieldX_gu

;       multiplies probfunc to magnetic field in the x direction

RCL Ion_BfieldY_gu RCL probfunct * STO Ion_BfieldY_gu

;       multiplies probfunc to magnetic field in the y direction

RCL Ion_BfieldZ_gu RCL probfunct * STO Ion_BfieldZ_gu

;       multiplies probfunc to magnetic field in the z direction

EXIT

    ;--------------------- done ----------------------------------------
```

Appendix B

6.7 Radiabeam Cad Drawing

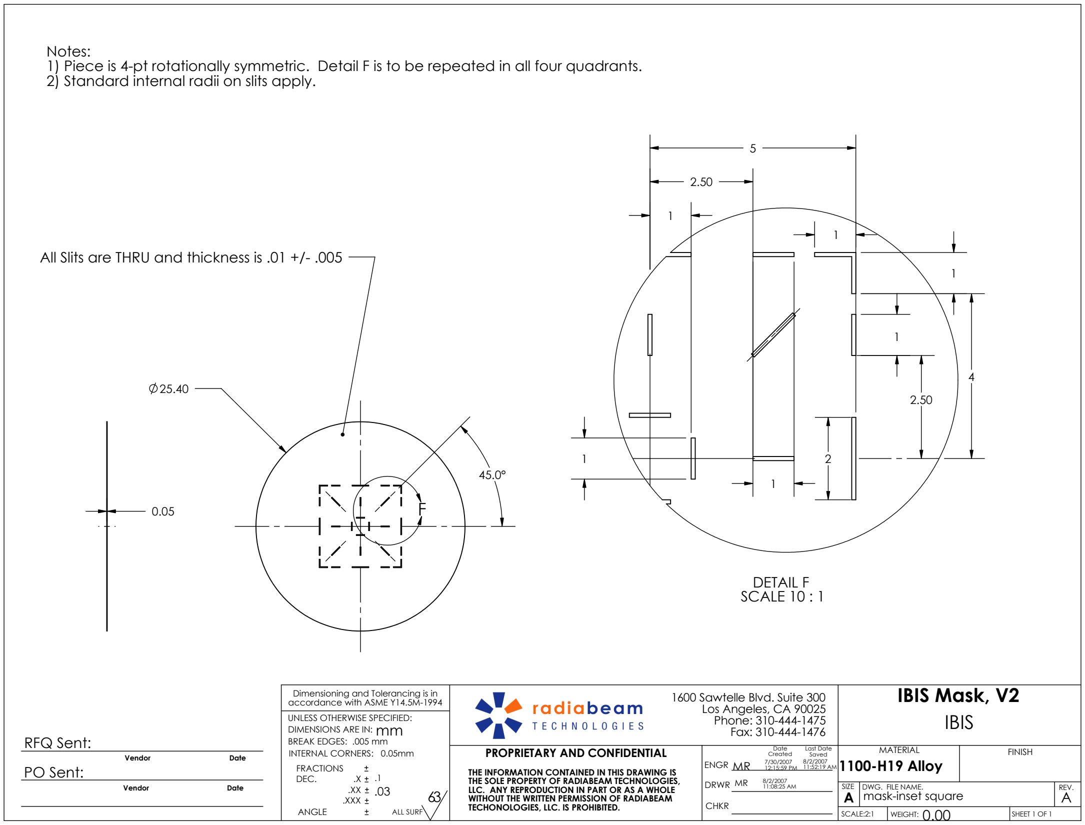
Notes:
1) Piece is 4-pt rotationally symmetric. Detail F is to be repeated in all four quadrants.
2) Standard internal radii on slits apply.

All Slits are THRU and thickness is .01 +/- .005

Dimensioning and Tolerancing is in accordance with ASME Y14.5M-1994
UNLESS OTHERWISE SPECIFIED:
DIMENSIONS ARE IN: mm
BREAK EDGES: .005 mm
INTERNAL CORNERS: 0.05mm
FRACTIONS ±
DEC. .X ± .1
.XX ± .03
.XXX ±
ANGLE ±

1600 Sawtelle Blvd. Suite 300
Los Angeles, CA 90025
Phone: 310-444-1475
Fax: 310-444-1476

PROPRIETARY AND CONFIDENTIAL

THE INFORMATION CONTAINED IN THIS DRAWING IS THE SOLE PROPERTY OF RADIABEAM TECHNOLOGIES, LLC. ANY REPRODUCTION IN PART OR AS A WHOLE WITHOUT THE WRITTEN PERMISSION OF RADIABEAM TECHONOLOGIES, LLC. IS PROHIBITED.

		Date Created	Last Date Saved
ENGR	MR	7/30/2007 12:15:59 PM	8/2/2007 11:52:19 AM
DRWR	MR	8/2/2007 11:08:25 AM	
CHKR			

IBIS Mask, V2
IBIS

MATERIAL: 1100-H19 Alloy
FINISH:
SIZE: A
DWG. FILE NAME. mask-inset square
REV. A
SCALE:2:1
WEIGHT: 0.00
SHEET 1 OF 1

RFQ Sent:
Vendor Date
PO Sent:
Vendor Date

Figure 6.1 CAD drawing, provided by RadiaBeam Technologies, of the aluminum mask

Appendix C

6.8 Wiring Diagrams

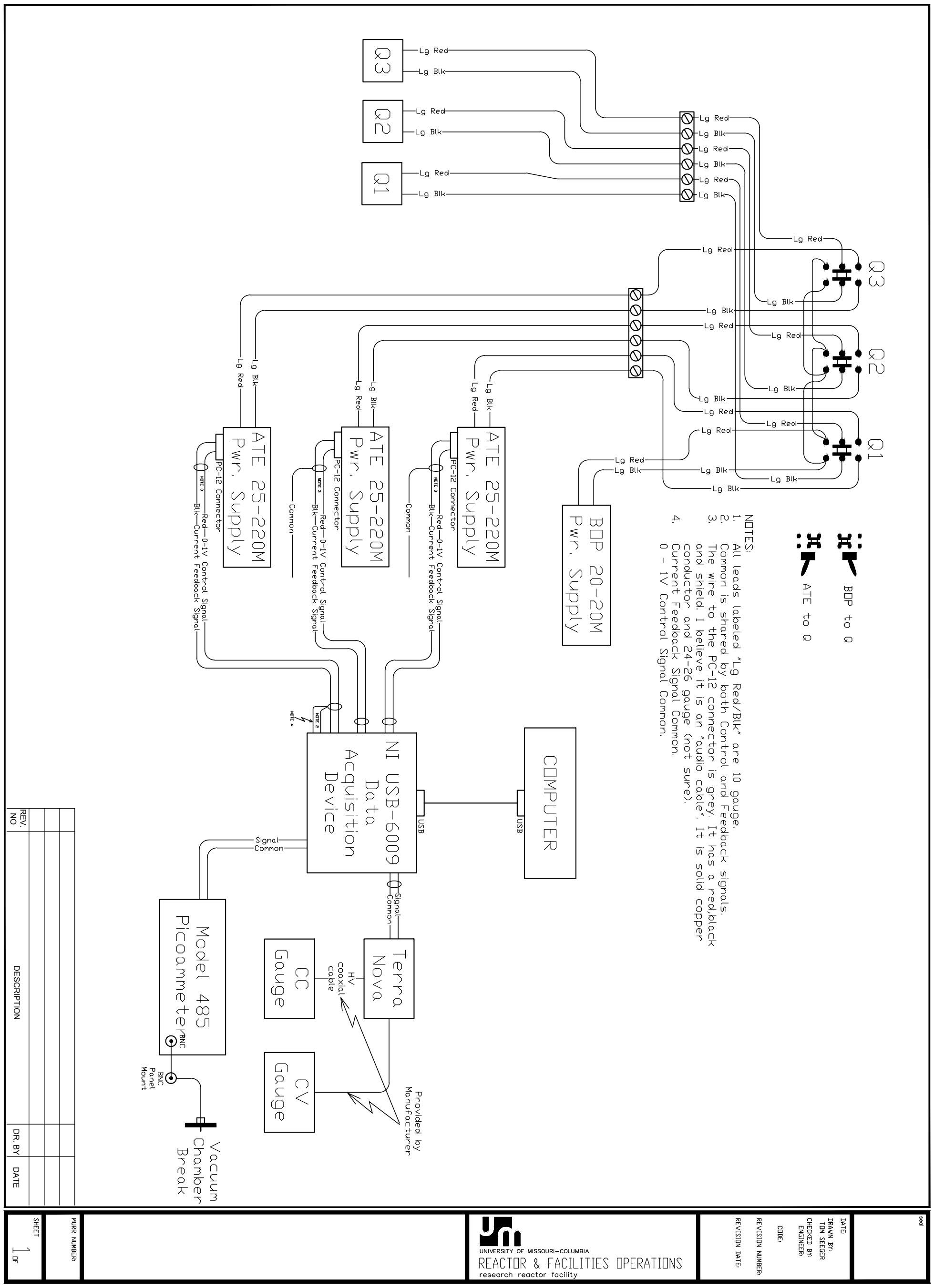

NOTES:
1. All leads labeled "Lg Red/Blk" are 10 gauge.
2. Common is shared by both Control and Feedback signals.
3. The wire to the PC-12 connector is grey. It has a red,black and shield. I believe it is an "audio cable". It is solid copper conductor and 24-26 gauge (not sure).
4. Current Feedback Signal Common.
0 - 1V Control Signal Common.

Figure 6.2 Wiring diagram-Instrumentation control and data acquisition.

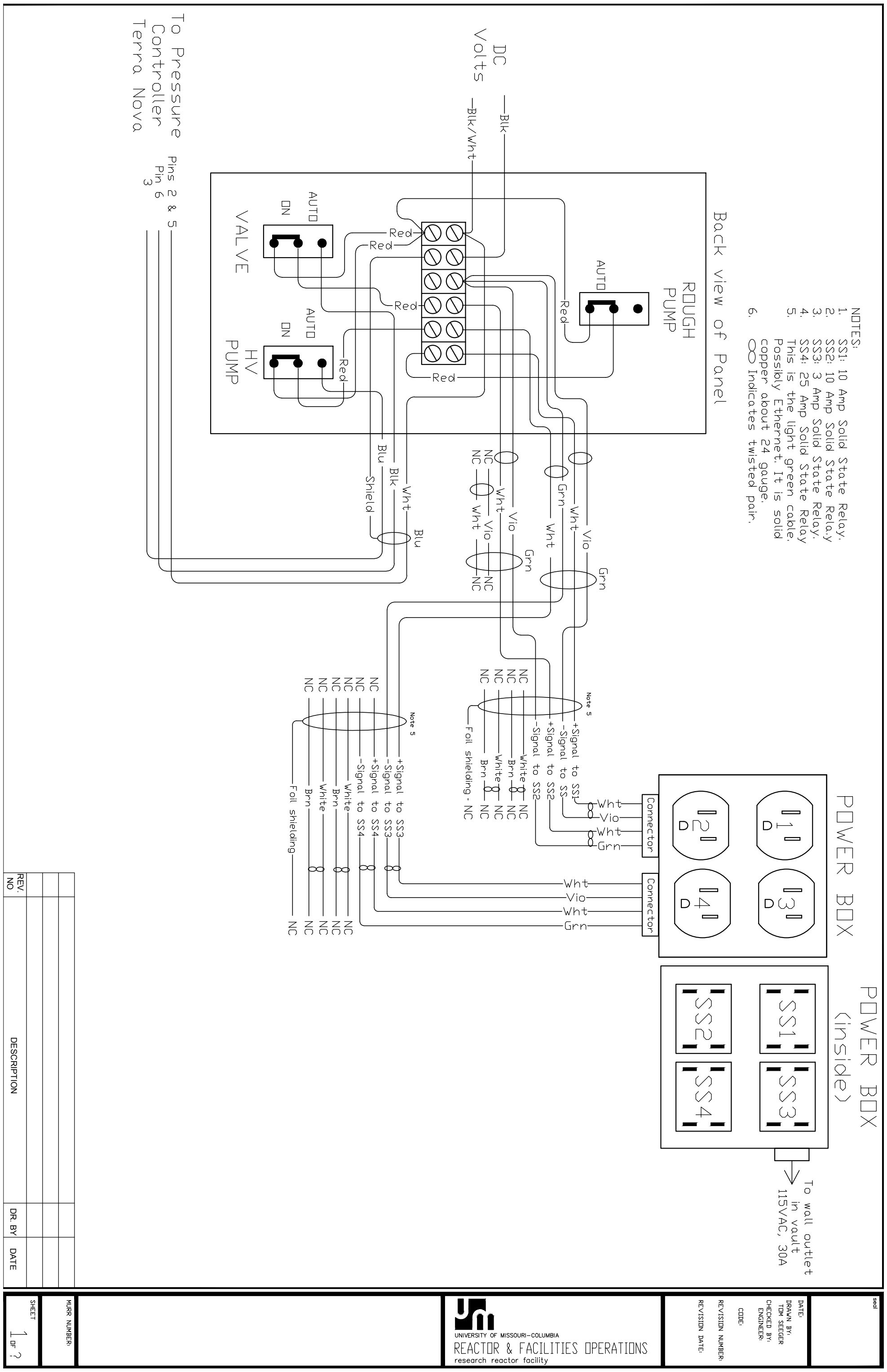

Figure 6.3   Wiring Diagram-Solid state relay box and switch panel.

6.9 Beamline Standard Operating Procedures

STARTUP - This should be done > 24 hours before an experiment

1) Turn on high vacuum system
    a) Turn on the NESLAB Chiller
        i) Make sure the set point is at 24°C
        ii) Make sure the NESLAB chiller is full of water (DI water)
    b) Turn on the two power strips in the bottom of the electronics tower.
    c) Turn on the mechanical pump
    d) Turn the oil diffusion pump to auto
        i) Make sure set point 1 High on the TerraNova pressure controller is: $5x10^{-2}$ torr
        ii) Make sure set point 1 LOW on the TerraNova pressure controller is: $5x10^{-3}$ torr
    e) Make sure the VAT valve is OFF
        i) Make sure the beamline is attached to the cyclotron and VAT valve
        ii) Make sure set point 2 High on the TerraNova pressure controller is: $5x10^{-3}$ torr
        iii) Make sure set point 2 LOW on the TerraNova pressure controller is: $5x10^{-4}$ torr
2) Intro Sample
    a) Isolate the vacuum chamber
        i) Close VAT valve
        ii) Close Al gate valve below vacuum chamber
    b) Turn off cold cathode pressure gauge
    c) Remove the top KF40 clamp from the KF40 tee between the VAT valve and vacuum chamber
    d) Backfill the chamber
    e) Remove the screws from the vacuum chamber lid
        i) Remove chamber lid - **be careful when removing the lid as there may be wires connected to the inside of the chamber**
    f) Mount sample
        i) Hook-up the current clamp, if desired
    g) Replace lid
        i) Make sure gasket is in grove
        ii) Screw lid to vacuum chamber
    h) Stop backfilling chamber
    i) Reattach the KF40 clamp
    j) Isolate the oil diffusion pump
        i) Close the gate valve between the oil diffusion pump and the roughing pump
    k) Bring vacuum chamber to high vacuum
        i) Open the bypass gate valve on the side of the vacuum chamber
        ii) Open the VAT valve.

        - iii) Wait 5 minutes
        - iv) Close the bypass gate valve
        - v) Open the gate valve between the oil diffusion pump and the roughing pump
        - vi) Open the gate valve between the oil diffusion pump and the vacuum chamber
    - l) Turn on the cold cathode pressure gauge
    - m) Make sure system reaches high vacuum (1x10^{-5} torr)

The system is now ready for the beam to be turned on. In the current configuration the mechanical pump is ON, the oil diffusion pump AUTO, and the VAT valve is ON. The VAT valve can be switched to auto, and then the TerraNova pressure controller will control it.

Beamline Operation

1) Make sure the vacuum chamber is under high vacuum (<1x10^{-5} torr)
2) Install camera in cyclotron vault
    - a) Plug USB connector into camera
    - b) Plug USB hub into computer
        - i) Make sure the USB hub power supply is plugged in
    - c) Open camera program
        - i) Make sure the vacuum chamber viewport is centered in the camera
        - ii) Adjust the camera position, as needed, to center the viewport
        - iii) Turn the lights off in the vault
3) Have the cyclotron operator startup the cyclotron
    - a) NOT the BEAM
4) Electronics Rack setup
    - a) Turn on Keithley
    - b) Make sure the three magnet switches are in the OFF position (Middle)
    - c) Make sure the Kepco voltage supply knobs are full counter clockwise
5) LabVIEW setup
    - a) Plug in the NI cards to their connectors.
        - i) The bottom of the NI cards are color coded to the connectors
    - b) Open the LabVIEW program
        - i) Set the file name and path where the WRITE file will be saved
        - ii) Click RUN and start the LabVIEW program
        - iii) Turn on the Kepco power supplies
            - (1) You will see a spike on the current output of the power supplies, this is normal
        - iv) Switch the quadrupole magnets switches to the ATE power supply source (DOWN position)
        - v) Make sure the quadrupole LabVIEW controls are set to 0,0, and 0.

        - vi) Rotate the voltage knobs on the Kepco power supplies fully clockwise
        - vii) In the program, make sure you can see the vacuum chamber pressure, beam current, and the current from the power supplies

6) Start experiment
    - a) Make sure operator is ready to turn on the beam
    - b) Begin capturing images with the camera program
    - c) Click WRITE in the LabVIEW program (should turn green)
    - d) Politely as the cyclotron operator to turn on the beam
        - i) The beam should be at low current 1st
        - ii) Make sure you see the beam in the camera
7) Focus Beam
    - a) In LabVIEW, adjust each quadrupole by **NO MORE THAN 0.1 V** at a time
        - i) Generally the beam is focused at set points
            - (1) Q1: 0.21V
            - (2) Q2: 0.31V
            - (3) Q3: 0.31V
    - b) Observe the beam image in the camera program
        - i) Remember you can adjust the gain and amount light the camera gets using the camera program
            - (1) This is very useful when the camera is saturated due to the beam being focused
        - ii) Make minor adjustments to the beam until you are happy
8) Bring cyclotron to operational current
    - a) Have the operator turn up the beam current
9) Shutdown
    - a) Have the operator turn off the beam
    - b) Stop recording in the camera program
    - c) Stop WRITING in the LabVIEW program
    - d) Close the LabVIEW program
    - e) Close the camera program
10) Sample removal
    - a) Work closely with HP and the cyclotron operator to do this in a SAFE manor

Appendix D

6.10 Tables and Figures for Beamline Alignment and Characterization

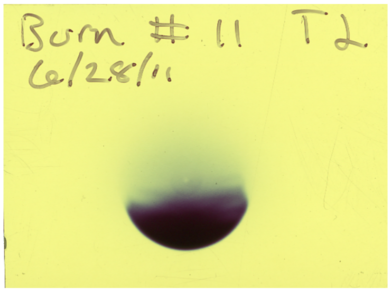

Figure 6.4 Image of the cyclotron beam using radiochromic film. Image taken on June 28th, 2011.

Table 6.1 Beam measurement experimental array on August 15st, 2011.

Sample #	Stripping Foil Position (%)	Foil Current (uA)	Target (uA)	Collimator 1/2 (uA)	Collimator 2/3 (uA)	Cyclotron Pressure (mbar)	Irradiation Time (s)	Setup
Burn 1	53.1	N/A	0.3	0	0.9	N/A	N/A	**1,2**
Burn 2	54.1	N/A	0.3	0	0.8	N/A	N/A	**1,2**
Burn 3	54.1	N/A	0.3	0	0.7	N/A	N/A	**1,3**
Burn 4	54.1	N/A	0.2	0	0.7	N/A	N/A	**1,3**
Burn 5	54.1	N/A	0.3	0	0.7	N/A	N/A	**1,3**
Burn 6	54.1	N/A	0.3	0	0.8	N/A	N/A	**1,3**
Burn 7	54.1	N/A	0.3	0	0.7	N/A	N/A	**1,3**
Burn 8	54.1	N/A	0.3	0	0.7	N/A	N/A	**1,3**
Burn 9	54.1	N/A	0.4	0	0.8	N/A	N/A	**1,3**

Setup: **1**-No collimator
2-Beam image taken after KF40 cyclotron adapter
3-Beam image taken after the short drift tube

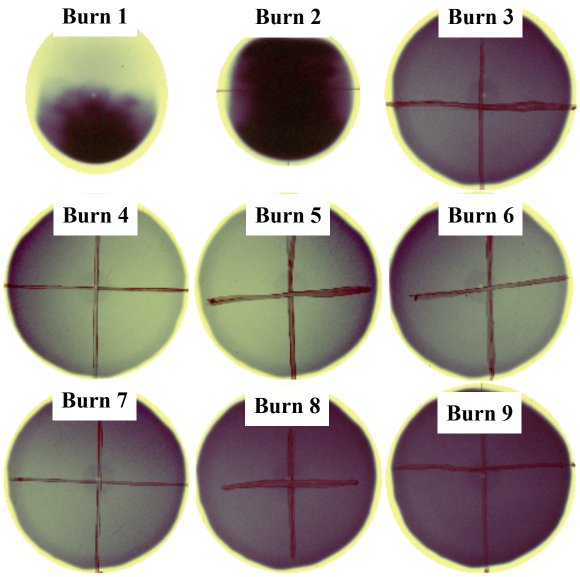

Figure 6.5 Images of the cyclotron beam using radiochromic film. Images taken on August 15th, 2011.

Table 6.2 Beam measurement experimental array on August 31st, 2011.

Sample #	Stripping Foil Position (%)	Foil Current (uA)	Target (uA)	Collimator 1/2 (uA)	Collimator 2/3 (uA)	Cyclotron Pressure (mbar)	Irradiation Time (s)	Setup
B1	52.0	N/A	6.0	1.2	0.1	1.40E-05	5	**1,2**
B1-2	52.0	N/A	6.3	1.2	0.2	1.30E-05	8	**1,2**
B1-3	52.0	N/A	6.0	1.4	0.1	1.30E-05	11	**1,2**
R1.1	52.0	N/A	1.0	0.2	0.0	1.40E-05	pulsed	**1,2**
R1.2	52.0	N/A	1.0	0.1	0.0	1.30E-05	pulsed	**1,2**
R1.3	52.0	N/A	1.0	0.2	0.0	1.30E-05	pulsed	**1,2**
R1.4	52.0	N/A	1.0	0.2	0.0	1.30E-05	5	**1,2**
B2	53.0	N/A	6.2	0.5	0.6	1.30E-05	10	**1,2**
R2.1	53.0	N/A	1.0	0.1	0.1	1.40E-05	2	**1,2**
R2.2	53.0	N/A	1.0	0.1	0.1	1.30E-05	5	**1,2**
R2.3	53.0	N/A	1.0	0.1	0.1	1.30E-05	5	**1,2**
B3	54.0	N/A	4.3	0.0	1.3	1.30E-05	5	**1,2**
B3-2	54.0	N/A	4.0	0.1	1.3	1.30E-05	10	**1,2**
B3-3	54.0	N/A	4.4	0.1	1.3	1.20E-05	12	**1,2**
R3-1	54.0	N/A	1.0	0.0	0.2	1.30E-05	5	**1,2**
R3.2	54.0	N/A	0.7	0.0	0.2	1.40E-05	pulsed	**1,2**
R3.3	54.0	N/A	0.7	0.0	0.2	1.30E-05	pulsed	**1,2**

Setup: **1**-No collimator
2-Beam image taken after KF40 cyclotron adapter

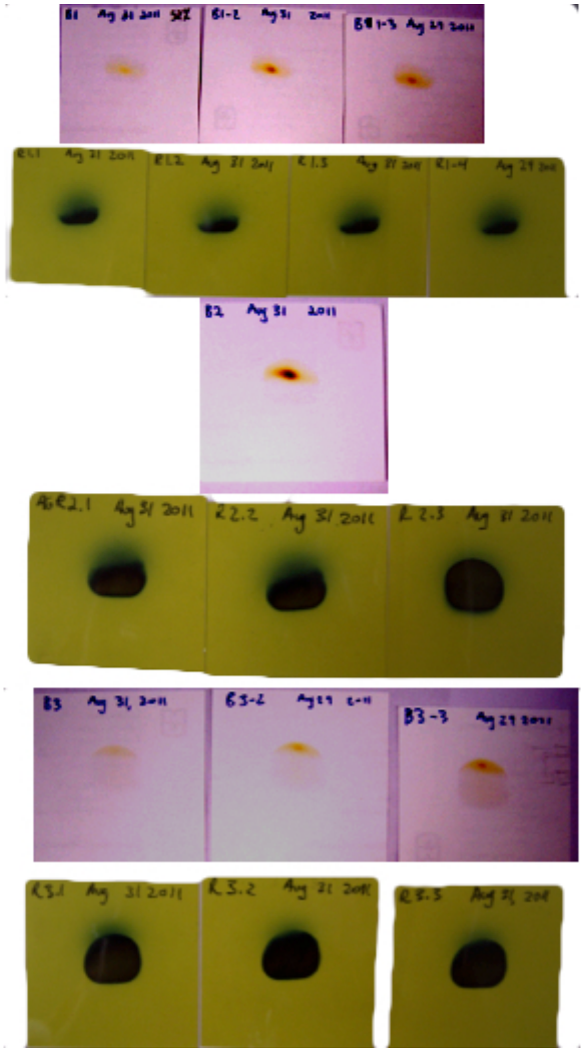

Figure 6.6 Images of the cyclotron beam using paper and radiochromic film. Images taken on August 31th, 2011.

Table 6.3 Beam measurement experimental array on September 19th, 2011.

Sample #	Stripping Foil Position (%)	Foil Current (uA)	Target (uA)	Collimator 1/2 (uA)	Collimator 2/3 (uA)	Cyclotron Pressure (mbar)	Irradiation Time (s)	Setup
R1	51	N/A	1.3	0.2	0.3	1.50E-05	5	**1,3**
R2	51	N/A	1.3	0.1	0.3	1.50E-05	5	**2,3**
R3	52	N/A	1.1	0	0.6	1.50E-05	5	**2,3**
R4	51	N/A	1.3	0.1	0.3	1.50E-05	5	**2,3**
R5	51	N/A	1.3	0.1	0.3	1.50E-05	10	**1,3**
R6	51	N/A	1.3	0.1	0.3	1.50E-05	10	**1,3**
R7	51	N/A	1.3	0.1	0.3	1.50E-05	10	**1,3**
R8	52	N/A	1.1	0	0.6	1.50E-05	10	**1,3**
R9	52	N/A	1.1	0	0.6	1.50E-05	10	**1,3**
R10	52	N/A	1.1	0	0.6	1.50E-05	10	**2,3**
R11	52	N/A	1.1	0	0.6	1.50E-05	10	**2,3**

Setup: **1**-No collimator
2-Collimator diameter is1mm
3-Beam image taken after the short drift tube

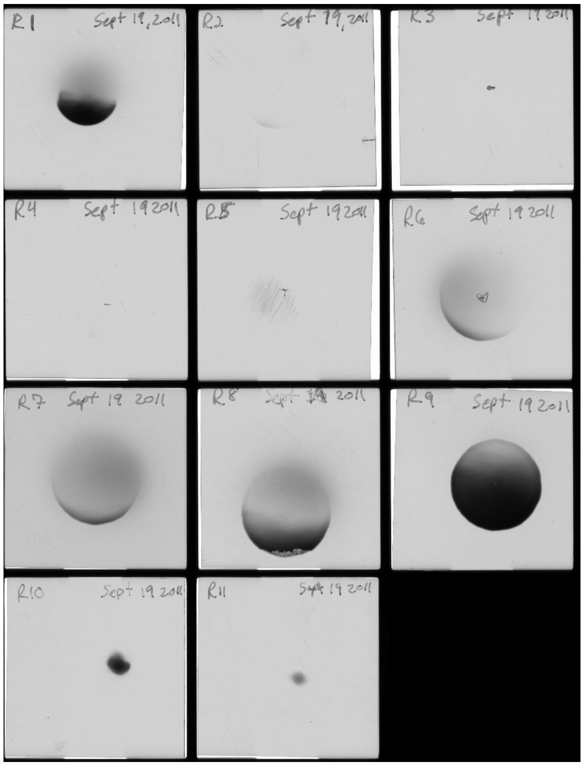

Figure 6.7 Images of the cyclotron beam using radiochromic film. Images taken on September 19th, 2011.

Table 6.4 Beam measurement experimental array on September 27th, 2011.

Sample #	Stripping Foil Position (%)	Foil Current (uA)	Target (uA)	Collimator 1/2 (uA)	Collimator 2/3 (uA)	Cyclotron Pressure (mbar)	Irradiation Time (s)	Setup
B1	52	N/A	1.4	0	0.4	1.30E-05	10	**1,2**
B2	52	N/A	1.5	0	0.4	1.30E-05	10	**1,2**
B3	52	N/A	1.7	0	0.4	1.30E-05	pulse	**1,2**
B4	52	N/A	1.6	0	0.5	1.30E-05	10	**1,2**
B5	52	N/A	1.6	0	0.5	1.30E-05	10	**1,2**
B6	52	N/A	1.6	0	0.5	1.30E-05	10	**1,2**
B7	52	N/A	1.6	0	0.5	1.30E-05	10	**1,2**
B8	52	N/A	1.6	0	0.5	1.30E-05	10	**1,2**
B9	52	N/A	1.6	0	0.5	1.30E-05	10	**1,2**
B10	52	N/A	1.6	0	0.5	1.30E-05	10	**1,2**
B11	52	N/A	1.6	0	0.5	1.30E-05	10	**1,2**
F1	52	N/A	1.5	0	0.5	1.30E-05	10	**1,3**
F2	52	N/A	1.5	0	0.5	1.30E-05	10	**1,3**

Setup: **1**-Collimator diameter is 0.5 mm
2-Beam image taken after the short drift tube
3-Beam image taken after the long drift tube

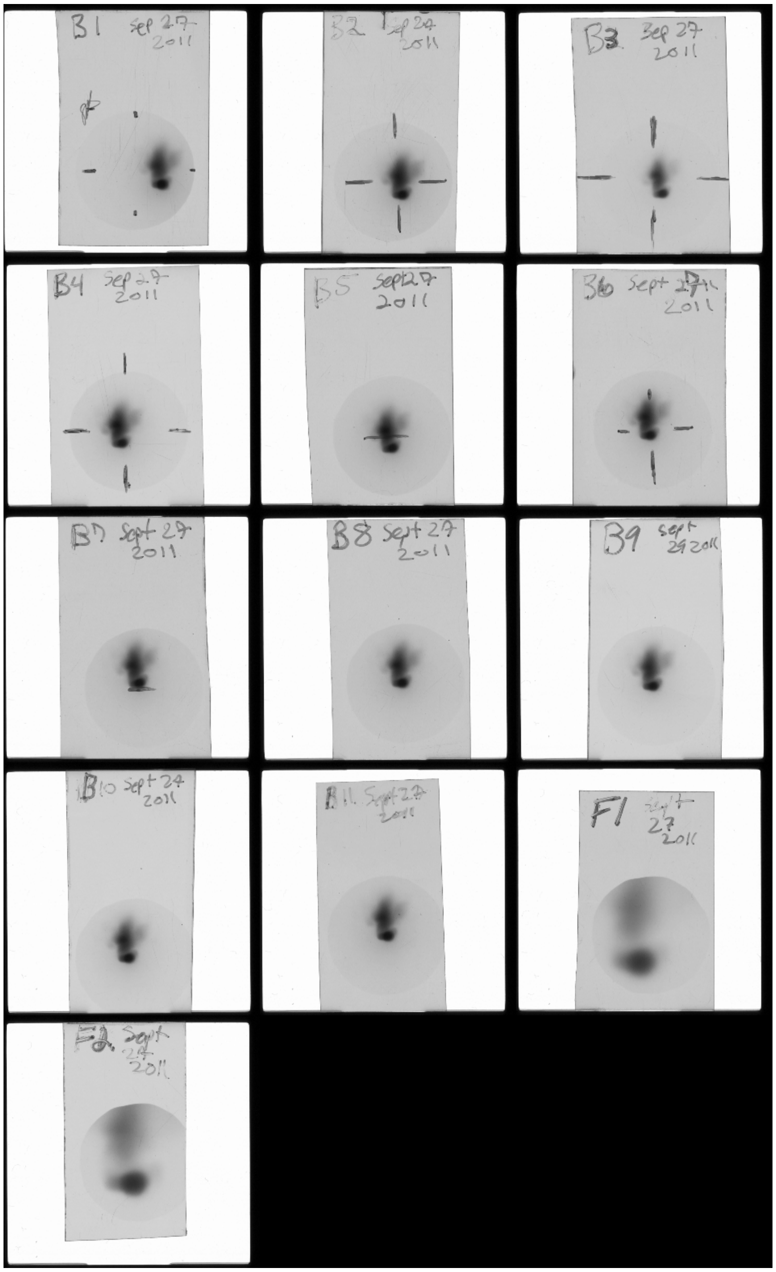

Figure 6.8 Images of the cyclotron beam using radiochromic film. Images taken on September 27th, 2011.

Table 6.5 Beam measurement experimental array on September 28th, 2011.

Sample #	Stripping Foil Position (%)	Foil Current (uA)	Target (uA)	Collimator 1/2 (uA)	Collimator 2/3 (uA)	Cyclotron Pressure (mbar)	Irradiation Time (s)	Setup
A1	52	N/A	1.5	0	0.4	1.30E-05	10	**1,4**
A2	52	N/A	1.6	0.1	0.3	1.30E-05	10	**1,4**
A3	52	N/A	1.6	0.1	0.3	1.30E-05	pulsed	**1,4**
A4	52	N/A	1.7	0.1	0.4	1.30E-05	10	**1,4**
A5	52	N/A	1.7	0.1	0.4	1.30E-05	10	**1,3**
A6	52	N/A	1.2	0.1	0.2	1.30E-05	pulse	**1,3**
A7	52	N/A	1	N/A	N/A	1.30E-05	pulse	**1,2**
A8	53	N/A	0.8	0	0.6	1.30E-05	pulse	**1,2**
A9	53	N/A	0.8	0	0.6	1.40E-05	pulse	**1,4**
A10	51	N/A	1.2	0.1	0.1	1.40E-05	pulse	**1,4**
A11	50	N/A	1.3	0.3	0.1	1.40E-05	pulse	**1,4**

Setup: **1**-Collimator diameter is 0.5 mm
2-Beam image taken after the collimator
3-Beam image taken after the short drift tube
4-Beam image taken after the long drift tube

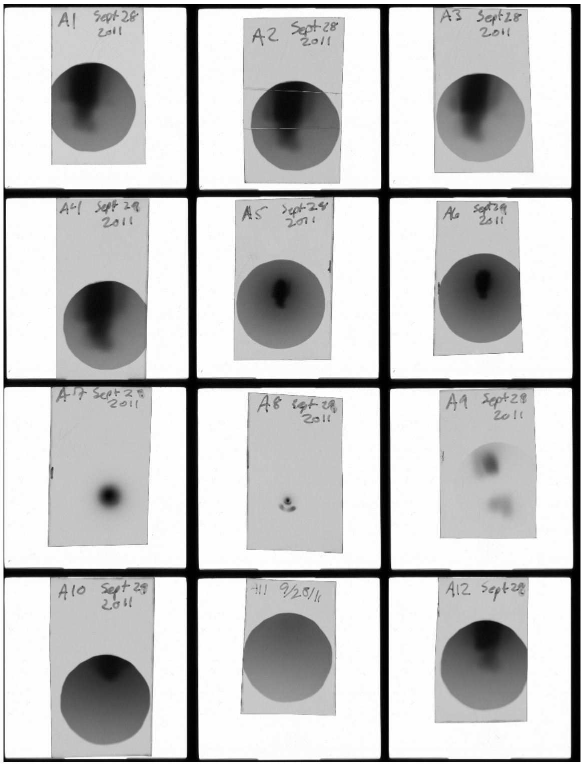

Figure 6.9 Images of the cyclotron beam using radiochromic film. Images taken on September 28th, 2011.

Table 6.6 Beam measurement experimental array on September 29th, 2011.

Sample #	Stripping Foil Position (%)	Foil Current (uA)	Target (uA)	Collimator 1/2 (uA)	Collimator 2/3 (uA)	Cyclotron Pressure (mbar)	Irradiation Time (s)	Setup
C1	52	N/A	1.4	0	0.4	1.30E-05	10	**1,3**
C2	52	1.9	1.5	0	0.4	1.30E-05	pulse	**1,3**
C3	53	1.96	1	0	0.9	1.30E-05	pulse	**1,3**
C4	52.5	1.97	1.4	0	0.5	1.30E-05	pulse	**1,3**
C5	52	1.2	0.89	0	0.2	1.30E-05	pulse	**1,3**
C6	52.2	1.2	0.7	0	0.3	1.30E-05	pulse	**1,3**
C7	50	1.9	1.6	0.2	0	1.30E-05	pulse	**1,3**
C8	51	1.97	1.67	0.1	0.1	1.30E-05	pulse	**1,3**
C9	52.4	1.97	1.56	0	0.5	1.30E-05	pulse	**1,3**
C10	52	0.75	0.62	0	0.2	1.30E-05	pulse	**2,3**
C11	53	0.72	0.47	0	0.3	1.30E-05	pulse	**2,3**
C12	51	N/A	0.56	0.1	0	1.30E-05	pulse	**2,3**

Setup: **1**-Collimator diameter is 0.5 mm
2-Collimator diameter is 3 mm
3-Beam image taken after the long drift tube

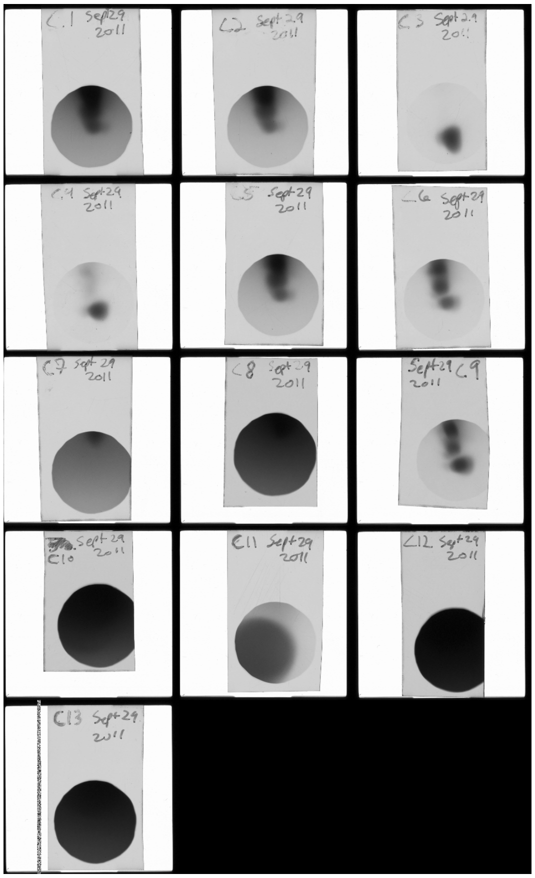

Figure 6.10 Images of the cyclotron beam using radiochromic film. Images taken on September 29th, 2011.

Table 6.7 Beam measurement experimental array on October 7th, 2011.

Sample #	Stripping Foil Position (%)	Foil Current (uA)	Target (uA)	Collimator 1/2 (uA)	Collimator 2/3 (uA)	Cyclotron Pressure (mbar)	Irradiation Time (s)	Setup
Q1	52	14.2	11.7	0.2	2.1	1.40E-05	10	**2,3**
X1	52	1.1	0.9	0	0.2	1.40E-05	3	**2,3**
X2	52	1.2	0.9	0	0.3	1.40E-05	pulse	**2,3**
X3	52	1.2	0.9	0	0.3	1.40E-05	pulse	**2,3**
X4	52	1.3	1	0	0.2	1.40E-05	pulse	**2,3**
X5	52	1.2	1	0	0.3	1.40E-05	pulse	**1,4**
X6	52	1.3	0.9	0	0.3	1.40E-05	pulse	**1,4**
X7	52	1.3	1	0	0.3	1.40E-05	pulse	**1,4**
X8	52	1.2	0.9	0	0.3	1.40E-05	pulse	**1,4**

Setup: **1**-Collimator diameter is 0.5 mm
2-Collimator diameter is 3 mm
3-Beam image taken after the short drift tube
4-Beam image taken after the long drift tube

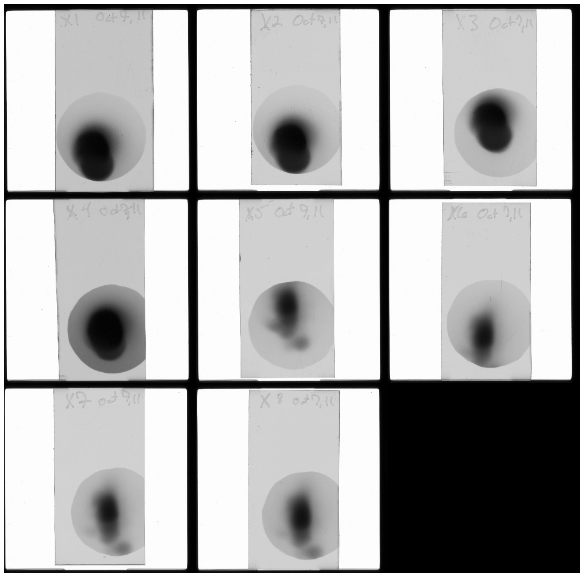

Figure 6.11 Images of the cyclotron beam using radiochromic film. Images taken on October 7th, 2011.

Table 6.8 Beam measurement experimental array on November 16th, 2011.

Stripping Foil Position (%)	Foil Current (uA)	Target (uA)	Collimator 1/2 (uA)	Collimator 2/3 (uA)	Cyclotron Pressure (mbar)	Irradiation Time (s)	Setup
50.5	1.02	0.58	0.5	0	NA	pulse	**1,2**
51	1.13	0.95	0.2	0	NA	pulse	**1,2**
51.5	1.08	0.87	0.1	0.1	NA	pulse	**1,2**
52	0.96	0.75	0.1	0.1	NA	pulse	**1,2**

Setup: **1**-Collimator diameter is 0.5mm
2-Beam image taken after the long drift tube

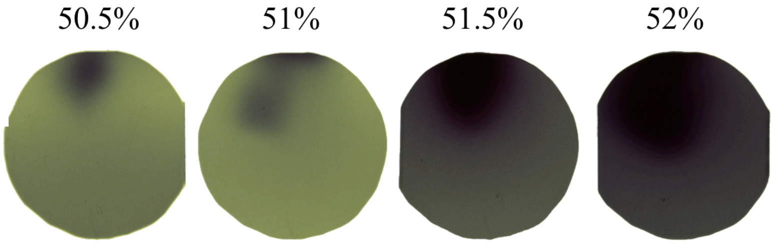

Figure 6.12 Images of the cyclotron beam using radiochromic film. Images taken on November 16th, 2011.

Table 6.9 Beam measurement experimental array on November 17th, 2011.

Stripping Foil Position (%)	Foil Current (uA)	Target (uA)	Collimator 1/2 (uA)	Collimator 2/3 (uA)	Cyclotron Pressure (mbar)	Irradiation Time (s)	Setup
52.2	0.4	0.37	0	0	NA	pulse	**1,2**
52.4	0.46	0.41	0	0	NA	pulse	**1,2**
52.5	0.5	0.45	0	0	NA	pulse	**1,2**
53	0.81	0.75	0	0.2	NA	pulse	**1,2**

Setup: **1**-Collimator diameter is 0.5mm
2-Beam image taken after the long drift tube

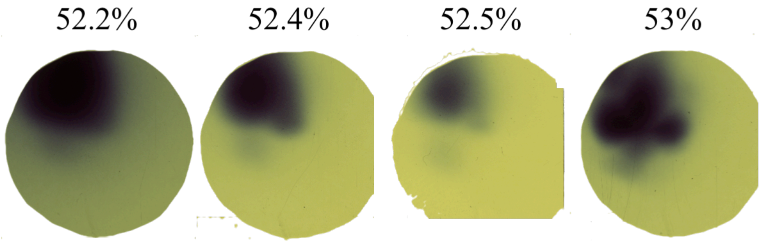

Figure 6.13 Images of the cyclotron beam using radiochromic film. Images taken on September 27th, 2011.

Table 6.10 Beam measurement experimental array on December 14th, 2011.

Sample #	Stripping Foil Position (%)	Foil Current (uA)	Target (uA)	Collimator 1/2 (uA)	Collimator 2/3 (uA)	Cyclotron Pressure (mbar)	Irradiation Time (s)	Setup
Short 1	52	1.16	1.03	0	0.1	1.30E-05	pulsed	**1**,**2**
Short 2	52	1.22	0.96	0	0.1	1.30E-05	pulsed	**1**,**2**
Long 1	52	1.02	0.86	0.00	0.10	1.70E-05	pulsed	**1**,**3**
Long 2	52	1.28	1.00	0.10	0.20	1.30E-05	pulsed	**1**,**3**
Long 3	52	1.28	1.14	0.10	0.20	1.30E-05	pulsed	**1**,**3**

Setup: **1**-Collimator diameter is 0.5mm
2-Beam image taken after the short drift tube
3-Beam image taken after the long drift tube

Table 6.11 Focused beam measurement experimental array on December 14th, 2011.

Sample #	Stripping Foil Position (%)	Foil Current (uA)	Target (uA)	Collimator 1/2 (uA)	Collimator 2/3 (uA)	Cyclotron Pressure (mbar)	Irradiation Time (s)	Setup
Long Mag 1	52	1.31	1.11	0.1	0.2	1.30E-05	pulsed	**1**,**3**
Long Mag 2	52	1.26	1.06	0.1	0.2	1.30E-05	pulsed	**1**,**3**
Long Mag 3	51.7	1.29	1.16	0.1	0.1	1.30E-05	pulsed	**1**,**3**
Long Mag 4	51.7	1.30	1.18	0.1	0.1	1.30E-05	pulsed	**1**,**3**
Long Mag 5	51.7	1.28	1.15	0.1	0.1	1.30E-05	pulsed	**1**,**3**
Long Mag 6	51.7	1.38	1.05	0.1	0.1	1.30E-05	pulsed	**1**,**3**
Long Mag 7	51.7	1.30	1.18	0.1	0.1	1.30E-05	pulsed	**1**,**3**
Long Mag 8	51.7	1.17	0.95	0.1	0.1	1.30E-05	pulsed	**2**,**3**
Long Mag 9	51.7	1.27	1.12	0.1	0.1	1.20E-05	pulsed	**2**,**3**
Long Mag 10	51.7	1.35	1.20	0.1	0.1	1.30E-05	pulsed	**2**,**3**
Long Mag 11	51.7	1.34	1.17	0.1	0.1	1.30E-05	pulsed	**2**,**3**

Setup: **1**-Collimator diameter is 0.5mm
2-No collimator
3-Beam image taken after the long drift tube

Table 6.12 Current of the quadrupoles for the focused beam measurement experimental array on December 14th, 2011.

Sample #	Stripping Foil Position (%)	Quadrupole #1 Current (A)	Quadrupole #2 Current (A)	Quadrupole #3 Current (A)	Setup
Long Mag 1	52	2.1	4.1	2.0	**1,3**
Long Mag 2	52	4.3	6.3	4.2	**1,3**
Long Mag 3	51.7	4.3	6.3	4.2	**1,3**
Long Mag 4	51.7	4.3	6.4	4.7	**1,3**
Long Mag 5	51.7	4.3	6.4	4.7	**1,3**
Long Mag 6	51.7	4.3	6.4	4.7	**1,3**
Long Mag 7	51.7	4.3	6.4	4.7	**1,3**
Long Mag 8	51.7	4.3	6.4	4.7	**2,3**
Long Mag 9	51.7	5.2	7.8	5.1	**2,3**
Long Mag 10	51.7	5.5	7.9	5.4	**2,3**
Long Mag 11	51.7	2.9	5.2	2.5	**2,3**

Setup: **1**-Collimator diameter is 0.5mm
2-No collimator
3-Beam image taken after the long drift tube

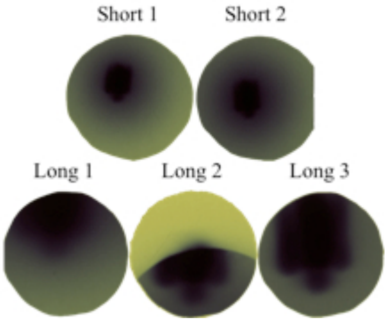

Figure 6.14 Images of the cyclotron beam using radiochromic film. Images taken on December 14th, 2011.

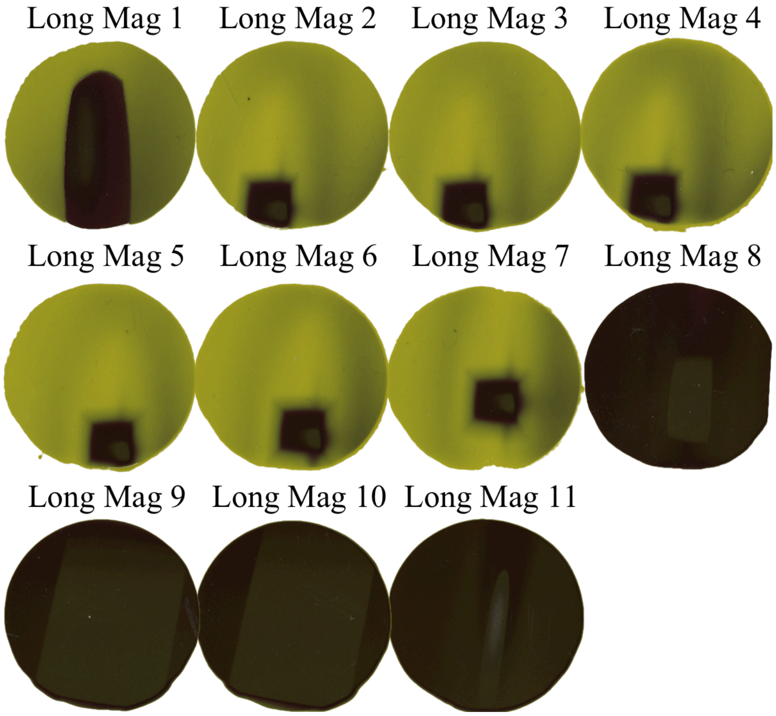

Figure 6.15 Images of the focused cyclotron beam using radiochromic film. Images taken on December 14th, 2011.